Chapter 2
Orbital Prediction Error Propagation of Space Objects

2.1 Definition of Coordinate System

In this section, we made a definition and description about all major coordinate systems mentioned in this book.

1. ECI coordinate system

Earth centered inertial (ECI) coordinate system is a common geocentric coordinate system [1, 2]. Its origin is at the center of the earth O_E, and the fundamental plane is the Earth's equator. The X axis is in the equatorial plane, pointing to the epoch mean vernal equinox; the Y axis is in the equatorial plane, at an angle of 90° to the east; the Z axis is vertical to the equatorial plane, coinciding with the earth's spin axis and pointing to the north pole. In view of the time-dependent nature of equator and ecliptic direction under the influence of precession and nutation, the International Astronomical Union (IAU) decided in 1976 to start applying the new epoch standard since 1984. The mean equinox at 12:00:00.00 on January 1st, 2000 has been taken as the benchmark. The coordinate system is also called J2000 ECI coordinate system.

2. Satellite-based orbit coordinate system

Satellite-based orbit coordinate system is the common system used to describe the relative motion of spacecraft, orbit prediction error, and orbital transfer. RSW and NTW coordinate systems [2] are the two common types of the satellite-based orbit coordinate system. Pay attention that there are different ways to define the orbit coordinate system, including the local vertical local horizontal (LVLH) coordinate system, the vehicle velocity local horizontal (VVLH) coordinate system, etc. They are the most common coordinate systems during space rendezvous and docking. In this book, we define the coordinate through Vallado's method [2].

The origin of RSW coordinate system is located at the centroid of the space object. The R axis (radial) always points from the Earth's center along the radius

L. Chen et al., *Orbital Data Applications for Space Objects*,
DOI 10.1007/978-981-10-2963-9_2

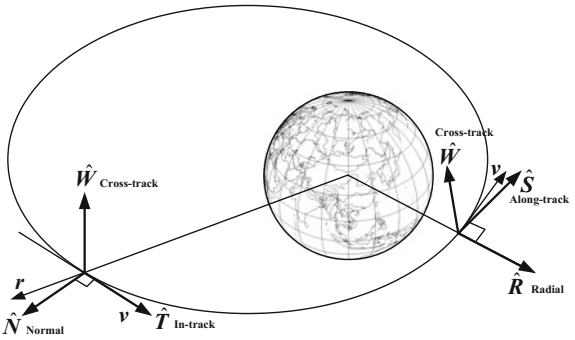

Fig. 2.1 Satellite-based RSW and NTW coordinate systems

vector toward the satellite as it moves through the orbit; the S axis (along-track or transverse) points in the direction of (but not necessarily parallel to) the velocity vector and is perpendicular to the radius vector; the W axis (cross-track) is normal to the orbital plane. Refer to Fig. 2.1 for details.

Sometimes, the coordinate system is also marked as RTN (radial, transverse, and normal) coordinate system or UVW coordinate system [3]. RSW coordinate system is decided by its position and velocity vectors, which vary with time. Its Axis S does not always coincide with the velocity direction. This kind of coordinate system is mainly used to describe orbital errors, relative position, and satellite orbital transfer of circular orbit.

In an ECI coordinate system, the unit vectors of the three axes of RSW coordinate system are $\hat{\boldsymbol{R}}$, $\hat{\boldsymbol{S}}$, and $\hat{\boldsymbol{W}}$ respectively.

$$\hat{\boldsymbol{R}} = \frac{\boldsymbol{r}}{|\boldsymbol{r}|}, \quad \hat{\boldsymbol{W}} = \frac{\boldsymbol{r} \times \boldsymbol{v}}{|\boldsymbol{r} \times \boldsymbol{v}|}, \quad \hat{\boldsymbol{S}} = \hat{\boldsymbol{W}} \times \hat{\boldsymbol{R}} \tag{2.1}$$

The transfer matrix between RSW coordinate system and ECI coordinate system is:

$$\boldsymbol{M}_{\mathrm{RSW}\to\mathrm{ECI}} = \begin{pmatrix} \hat{\boldsymbol{R}} & \hat{\boldsymbol{S}} & \hat{\boldsymbol{W}} \end{pmatrix}, \quad \boldsymbol{M}_{\mathrm{ECI}\to\mathrm{RSW}} = \begin{pmatrix} \hat{\boldsymbol{R}} & \hat{\boldsymbol{S}} & \hat{\boldsymbol{W}} \end{pmatrix}^{\mathrm{T}} \tag{2.2}$$

The origin of NTW coordinate system is in the centroid of the space orbit, Axis T (tangential or in-track) is tangent to the orbit and points to the velocity direction, Axis N (normal) is located in the orbital plane, vertical to the velocity direction, positive upward and its Axis W (cross-track) is vertical to the orbital place. Refer to Fig. 2.1 for details. NTW coordinate system also varies with its position and velocity. This kind of coordinate system is mainly used for the atmospheric damping impact analysis and error analysis of elliptical orbits.

In the ECI coordinate system, the unit vectors of the three axes of NTW coordinate system are $\hat{\boldsymbol{N}}$, $\hat{\boldsymbol{T}}$, and $\hat{\boldsymbol{W}}$ respectively.

$$\hat{\boldsymbol{T}} = \frac{\boldsymbol{v}}{|\boldsymbol{v}|}, \quad \hat{\boldsymbol{W}} = \frac{\boldsymbol{r} \times \boldsymbol{v}}{|\boldsymbol{r} \times \boldsymbol{v}|}, \quad \hat{\boldsymbol{N}} = \hat{\boldsymbol{T}} \times \hat{\boldsymbol{W}} \tag{2.3}$$

The transfer matrix between the NTW coordinate system and the ECI coordinate system is:

$$\boldsymbol{M}_{\mathrm{NTW}\to\mathrm{ECI}} = \begin{pmatrix} \hat{\boldsymbol{N}} & \hat{\boldsymbol{T}} & \hat{\boldsymbol{W}} \end{pmatrix}, \quad \boldsymbol{M}_{\mathrm{ECI}\to\mathrm{NTW}} = \begin{pmatrix} \hat{\boldsymbol{N}} & \hat{\boldsymbol{T}} & \hat{\boldsymbol{W}} \end{pmatrix}^{\mathrm{T}} \tag{2.4}$$

NTW coordinate system is also presented as UNW coordinate system. Its Axis U is tangent with orbit and points to velocity direction, Axis N is located in the orbital plane, vertical to the velocity direction, positive upward and its Axis W is vertical to the orbital plane. In the ECI coordinate system, the unit vectors of the three axes of UNW coordinate system are $\hat{\boldsymbol{U}}$, $\hat{\boldsymbol{N}}$, and $\hat{\boldsymbol{W}}$ respectively.

$$\hat{\boldsymbol{U}} = \frac{\boldsymbol{v}}{|\boldsymbol{v}|}, \quad \hat{\boldsymbol{W}} = \frac{\boldsymbol{v} \times \boldsymbol{r}}{|\boldsymbol{v} \times \boldsymbol{r}|}, \quad \hat{\boldsymbol{N}} = \hat{\boldsymbol{W}} \times \hat{\boldsymbol{U}} \tag{2.5}$$

$$\boldsymbol{M}_{\mathrm{UNW}\to\mathrm{ECI}} = \begin{pmatrix} \hat{\boldsymbol{U}} & \hat{\boldsymbol{N}} & \hat{\boldsymbol{W}} \end{pmatrix}, \quad \boldsymbol{M}_{\mathrm{ECI}\to\mathrm{UNW}} = \begin{pmatrix} \hat{\boldsymbol{U}} & \hat{\boldsymbol{N}} & \hat{\boldsymbol{W}} \end{pmatrix}^{\mathrm{T}}. \tag{2.6}$$

2.2 Overview of Orbital Prediction Errors

2.2.1 Category of Orbital Prediction Errors

The orbital problems mainly include three aspects: Orbital observation, orbital determination, and orbital prediction. Due to various inevitable factors, errors including measuring errors, modeling errors, and methodology errors may exist. The true value of orbit objectively exists, but is unknown. Any orbital measuring method may have errors. An error refers to a deviation and noise. We can only acquire the optimally approximate value of the true orbit value by determining and making assessments with the contaminated data.

Through orbital determination, we can get the initial mean value and initial covariance of the orbit at t0. The initial mean value of the orbit is not always equal to the true value. We can get the orbital prediction value and covariance prediction value through orbital propagation. Figure 2.2 is a schematic diagram of the error generation process during space object orbital determination and prediction.

Space object orbital prediction errors include initial errors and model errors. The object state vector at initial epoch time can be acquired through orbital determination after data (radar, photology, GPS, etc.) processing. Due to the errors in measured data, the state vector will inevitably have some errors which are also known as initial state errors. During orbital propagation, the initial state errors will diffuse along with the extrapolation of orbital model and its propagation characteristics and tendency will vary according to the types of orbits. Based on the

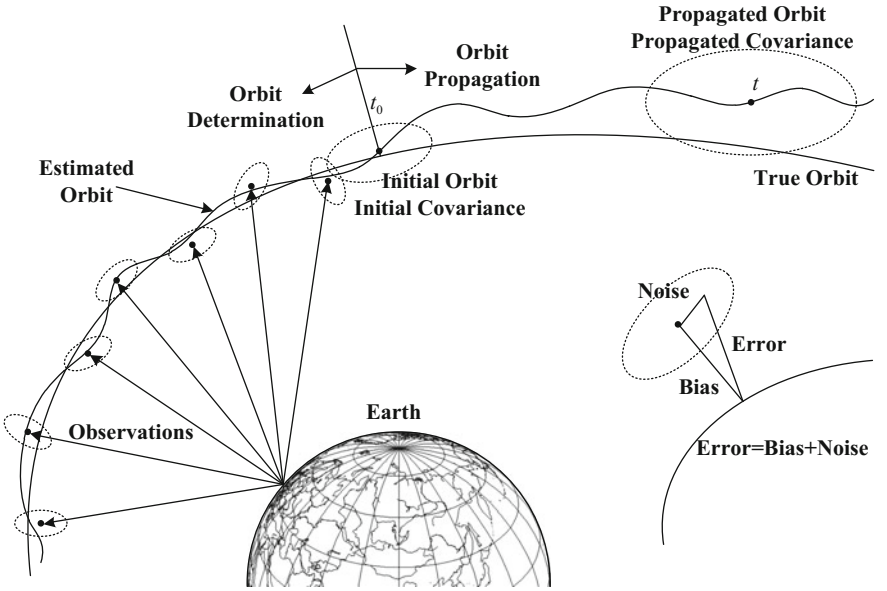

Fig. 2.2 Schematic diagram of errors during space object orbital determination and prediction

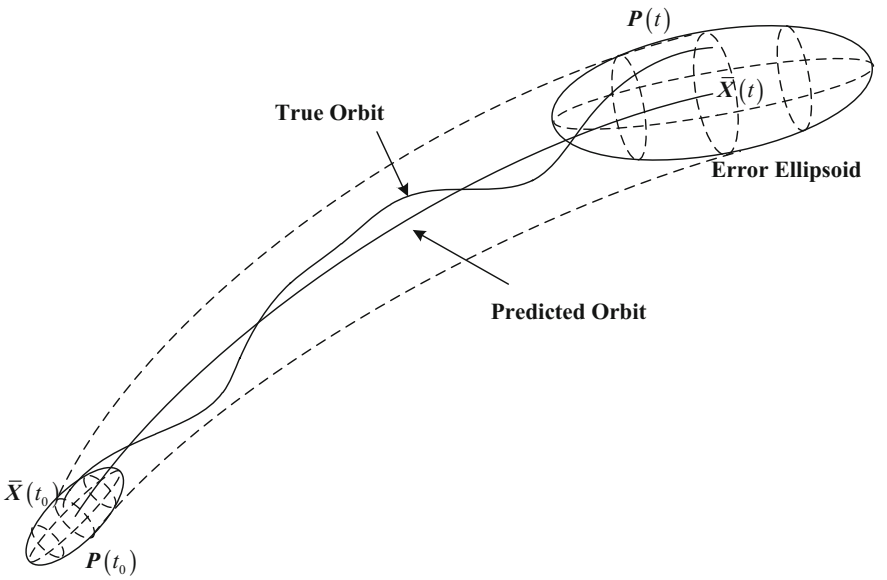

Fig. 2.3 Propagation of initial errors

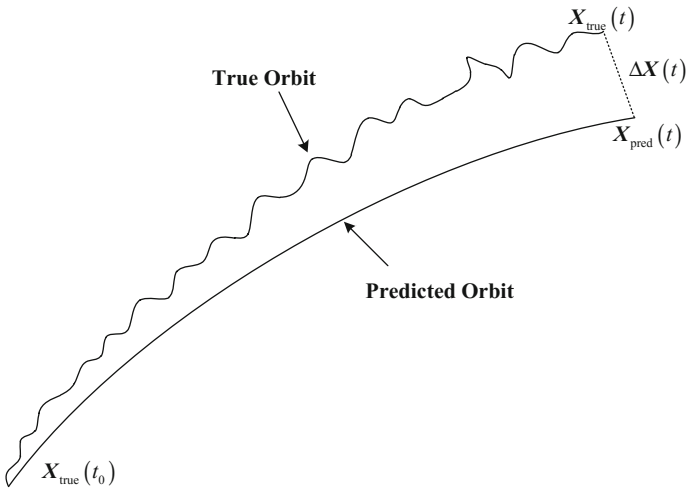

Fig. 2.4 Orbital model errors

propagation of orbital mean value and covariance, we can work out an error pipe in which the orbital true value exists at a high probability. Refer to Fig. 2.3.

The incompleteness of orbital propagation model can cause model errors during orbital propagation. If we can get the orbital true value at the initial time, model errors may bring about orbital propagation errors, refer to Fig. 2.4. The diffusion of initial errors and model errors may be coupled with each other. Orbital prediction error analysis is a complicated problem.

During orbital propagation, the magnitudes of initial errors are different from those of model errors. For the orbital propagation model with a relatively high precision, its initial errors will be much greater than the model errors. To simplify the analysis process, the analysis of initial errors is decoupled with that of the model errors. When analyzing initial errors, the orbital prediction model shall be regarded as correct without any model error and the propagation characteristics of initial errors will be obtained. When analyzing model errors, different models with the same initial state shall be taken for the orbital propagation, and the propagation results shall be compared with each other.

One of the major problems for object monitoring and space object orbital data application is acquiring the orbital propagation error covariance information of space object and knowing the precision of that information. In practice, we usually use the inner fitting precision and outer comparing precisions to define the precision of orbital determination [4]. Considering the two assessment methods and the actual engineering conditions, the analytical methods elaborated in the domestic and foreign literature are error extrapolation based on orbital models, comparison with high-precision orbital prediction results, and error analysis based on historical

orbital data in allusion to different objects and sources of their orbit information. In this chapter, we have a brief introduction about the first two methods. And the third method will be discussed in the next chapter.

2.2.2 Model-Based Orbital Error Propagation

For the space cooperative objects like the normal spacecraft owned or controlled by one's own side, the owner or operator of the spacecraft shall take the responsibility for the orbital determination, acquire the measured data with a relatively high precision by various means, obtain the orbital elements and motion state vector based on the orbital determination theories, and get the error information of orbital determination or initial covariance matrix. Initial covariance matrix propagation can be realized with transfer matrix which depends on the orbital model we used.

Due to the nonlinear dynamic orbit model, we cannot get the analytical transfer matrix. In addition to the numerical analysis method, covariance analysis describing function technique (CADET) is a common tool for linearization error analysis. The Analytic Sciences Corporation of U.S. put forward CADET to analyze the statistical properties of linear or nonlinear systems with random errors. This method is featured with the characteristics of time saving, high efficiency, and high reliability [5–8]. The basic concept of CADET is: firstly, we conduct the statistical linearization on the nonlinear system based on the describing function theory; then, work out the mean values of the random state variables and the covariance propagation differential equation of the linearized system based on CADET. Once the two differential equations are worked out, we can determine the statistical properties of system state variables through one-time solution. Therefore, compared with the sampling statistics method (Monte Carlo Method), CADET can save more time. In addition, we can get accurate solutions for linear system by applying CADET. For nonlinear systems, approximate values can also be obtained by means of statistical linearization.

Liang et al. put forward the CADET method for error propagation analysis [9, 10] in allusion to the rendezvous and docking issues. In view of the navigation and control errors, CADET propagation model for relative states and deviation statistical variables has been established based on the C-W equation. In view of the orbital perturbation model, navigation and control errors, the CADET propagation model for relative states and deviation statistical variables has been established by nonlinear perturbation dynamical equation.

We can get the error covariance matrix with a high precision through an orbital error propagation, which requires the covariance at initial time and orbit model with high precision. However, this is difficult to satisfy under normal circumstances. This method takes a long time for calculation and cannot be applied to a large batch of objects, so it is only applicable to some controllable cooperative objects. In general cases, we usually adopt the method for the generation of orbit propagation errors of key spacecrafts in space surveillance missions.

2.2.3 Comparison with High Precision Ephemeris

The orbital prediction precision can be evaluated by comparing the orbital prediction ephemeris with high precision ephemeris. Higher precision orbital data for reference are usually obtained from the owner of spacecraft, orbital determination observation, or data from the high precision orbital predictor. Vallado has done a relatively thorough comparison about the difference of each orbital prediction model [11, 12]. Chan compared the prediction results [13] of TLE prediction orbit and double-station ranging orbital determination system of Intelsat's geostationary orbital communication satellite group, analyzed the variation of errors with time, and gave out the different characteristics of errors over different marine areas. Kelso analyzed the TLE orbital prediction results and the high precision ephemeris of GPS satellites, as well as the consistency of TLE data [14]. Boyce also analyzed the TLE prediction errors of Iridium constellation [15]. Snow compared the precisions of TLE data and the corresponding measured date that are used to generate the TLE data [16]. Muldoon improved the orbital determination and propagation with GPS measured data [17]. Before and after the epoch time of TLE, estimated initial error at epoch time can be obtained by comparing the high precision orbital determination results with the TLE data to get the initial value for error propagation of the orbit.

For most users, this precision assessment method which can only be used for the result comparison and verification is inapplicable, as it is impossible to get the high precision orbital determination results of most objects in space catalogue and most users are incapable to get the measured data or high precision ephemeris. In addition, the orbital prediction error of each object is unique, requiring separate analysis. Few objects with high precision ephemeris cannot represent all objects on the same orbit completely.

2.3 Covariance Analysis Describing Function Technique

2.3.1 Covariance Analysis of Linear System

The differential equation of first order can be applied to the description of random system in a linear continuous time domain:

$$\dot{\boldsymbol{x}}(t) = \boldsymbol{F}(t)\boldsymbol{x}(t) + \boldsymbol{G}(t)\boldsymbol{w}(t) + \boldsymbol{D}(t) \tag{2.7}$$

Wherein: $\boldsymbol{x}(t)$ is the state vector of n-dimensional systems, which is composed of plenty of state variables that can describe the system state; $\boldsymbol{w}(t)$ is the m-dimensional disturbance and also the stochastic noise vector of the control input of the system; $\boldsymbol{F}(t)$ and $\boldsymbol{G}(t)$ are deterministic functional matrixes and $\boldsymbol{D}(t)$ is deterministic functional vector.

As random state $\boldsymbol{x}(t)$ is made up of mean value $\bar{\boldsymbol{x}}(t)$ and random component $\delta\boldsymbol{x}(t)$, the random system in a linear continuous time domain can be described as follow:

$$\boldsymbol{x}(t) = \bar{\boldsymbol{x}}(t) + \delta\boldsymbol{x}(t) \tag{2.8}$$

$$\bar{\boldsymbol{x}}(t) = E\{\boldsymbol{x}(t)\}, \quad \boldsymbol{P}(t) = E\left\{\delta\boldsymbol{x}(t)\delta\boldsymbol{x}^T(t)\right\} \tag{2.9}$$

Similarly, random noise vector $\boldsymbol{w}(t)$ is composed of mean value $\bar{\boldsymbol{w}}(t)$ and random component $\delta\boldsymbol{w}(t)$, the random system in a linear continuous time domain can be described as follows:

$$\boldsymbol{w}(t) = \bar{\boldsymbol{w}}(t) + \delta\boldsymbol{w}(t) \tag{2.10}$$

$$\bar{\boldsymbol{w}}(t) = E\{\boldsymbol{w}(t)\} \tag{2.11}$$

When the disturbance is white noise, the covariance matrix of process noise can be presented as:

$$E\left\{\delta\boldsymbol{w}(\tau)\delta\boldsymbol{w}^T(t)\right\} = \boldsymbol{Q}(t)\delta(t-\tau) \tag{2.12}$$

Wherein, $\delta(t-\tau)$ is the Dirac function, which has the following properties:

$$\delta(t-\tau) = \begin{cases} 0 & (t \neq \tau) \\ \infty & (t = \tau) \end{cases}, \int_{-\infty}^{\infty} \delta(\varsigma)\mathrm{d}\varsigma = 1 \tag{2.13}$$

According to the describing function theory of linear system, the equation set of mean value and covariance propagation is shown as follows:

$$\begin{cases} \dot{\bar{\boldsymbol{x}}}(t) = \boldsymbol{F}(t)\bar{\boldsymbol{x}}(t) + \boldsymbol{G}(t)\bar{\boldsymbol{w}}(t) + \boldsymbol{D}(t) \\ \dot{\boldsymbol{P}}(t) = \boldsymbol{F}(t)\boldsymbol{P}(t) + \boldsymbol{P}(t)\boldsymbol{F}^T(t) + \boldsymbol{G}(t)\boldsymbol{Q}(t)\boldsymbol{G}^T(t) \end{cases} \tag{2.14}$$

Wherein: the diagonal elements of covariance matrix are the mean square errors of the random parts of state variables and the off-diagonal elements describe the correlation among all state variables. The covariance matrix is composed of these two kinds of elements. Based on the mean value and the covariance propagation equation set, we can work out the statistical rules of system state variables. So we can get the state mean and variance at any time by knowing the initial conditions $\bar{\boldsymbol{x}}(t_0)$ and $\boldsymbol{P}(t_0)$. Second item of Eq. (2.14) is same as the linear system matrix Ricatti Equation [8].

2.3.2 Covariance Analysis of Nonlinear System

The differential equation for the nonlinear system in a continuous time domain:

$$\dot{\boldsymbol{x}}(t) = \boldsymbol{f}(\boldsymbol{x}, t) + \boldsymbol{G}(t)\boldsymbol{w}(t) + \boldsymbol{D}(t) \tag{2.15}$$

where $\boldsymbol{f}(\boldsymbol{x}, t)$ is a nonlinear vector function of the n-dimensional state variable $\boldsymbol{x}(t)$. Definitions of other functions are the same as the definitions in linear system.

For CADET method for nonlinear system, first of all, we shall conduct the statistical linearization on the nonlinear system by applying the describing function theory. Then, we need to analyze the statistic performance of the linear system by using the covariance analysis method.

With the purpose of turning the nonlinear function $\boldsymbol{f}(\boldsymbol{x},t)$ into the approximate linear function of state variable $\boldsymbol{x}(t)$, the linearization includes true linearization and quasi-linearization. Taylor series expansion method is the most common method in true linearization. Statistical linearization belongs to quasi-linearization. According to the probability density function form of state function $\boldsymbol{x}(t)$, statistical linearization is to use a linear function $\boldsymbol{f}(\boldsymbol{x})$ to approximate the nonlinear function within a large variation range of $\boldsymbol{x}(t)$. The nonlinear function $\boldsymbol{f}(\boldsymbol{x})$ is not required to be continuous and differentiable. This method makes the linearization of a large number of nonlinear functions possible, such as the step, saturation control, and numerical switch functions that are frequently used in flight vehicles, which cannot be linearized by using true linearization methods. Statistic linearization, however, has disadvantages. We have to know the form of the probability density function of $\boldsymbol{x}(t)$. Therefore, the same function with different probability density will have different linearization results.

Statistic linearization steps: for nonlinear vector function $\boldsymbol{f}(\boldsymbol{x}, t)$ of random state variable $\boldsymbol{x}(t)$, work out the quasi-linear equation $\hat{\boldsymbol{f}} + \boldsymbol{N}_{\delta x}\delta\boldsymbol{x}$ to minimize the mean square error $E\{\boldsymbol{e}^{\mathrm{T}}\boldsymbol{e}\}$ between this equation and vector function $\boldsymbol{f}(\boldsymbol{x}, t)$. Wherein:

$$\boldsymbol{e} = \boldsymbol{f} - \boldsymbol{N}_{\bar{x}}\bar{\boldsymbol{x}} - \boldsymbol{N}_{\delta x}\delta\boldsymbol{x} = \boldsymbol{f} - \hat{\boldsymbol{f}} - \boldsymbol{N}_{\delta x}\delta\boldsymbol{x} \tag{2.16}$$

Shall meet the:

$$\frac{\partial}{\partial \boldsymbol{N}_{\bar{x}}}\mathrm{tr}\left(E\left\{\boldsymbol{e}^{\mathrm{T}}\boldsymbol{e}\right\}\right) = \frac{\partial}{\partial \boldsymbol{N}_{\delta x}}\mathrm{trace}\left(E\left\{\boldsymbol{e}^{\mathrm{T}}\boldsymbol{e}\right\}\right) = 0 \tag{2.17}$$

Assume

$$\boldsymbol{N}_{\bar{x}}(\bar{\boldsymbol{x}}, \quad \boldsymbol{P})\bar{\boldsymbol{x}} = E\{\boldsymbol{f}(\boldsymbol{x}, t)\} \tag{2.18}$$

The describing function can be obtained,

$$\begin{aligned}\hat{\boldsymbol{f}}(t) &= E\{\boldsymbol{f}(\boldsymbol{x},t)\} \\ \boldsymbol{N}_{\delta\boldsymbol{x}}(t) &= E\{\boldsymbol{f}(\boldsymbol{x},t)\delta\boldsymbol{x}^{\mathrm{T}}(t)\}\boldsymbol{P}^{-1}(t)\end{aligned} \tag{2.19}$$

where $\boldsymbol{N}_{\delta\boldsymbol{x}}$ is known as a dynamic matrix of quasi-linear system; $\hat{\boldsymbol{f}}$ is the expectant vector which can be formulated as:

$$\hat{\boldsymbol{f}} = E\{\boldsymbol{f}(\boldsymbol{x},t)\} = \int_{-\infty}^{\infty} \boldsymbol{f}(\boldsymbol{x},t)p(\boldsymbol{x})\mathrm{d}\boldsymbol{x} \tag{2.20}$$

where $p(\boldsymbol{x})$ is the probability density function of $\boldsymbol{x}(t)$.

Statistic linearization theory shall be applied, i.e.,

$$\boldsymbol{f} \simeq \hat{\boldsymbol{f}} + \boldsymbol{N}_{\delta\boldsymbol{x}}\delta\boldsymbol{x} \tag{2.21}$$

Substitute the above equation into Eq. (2.15), we can get:

$$\begin{aligned}\dot{\boldsymbol{x}}(t) &= \hat{\boldsymbol{f}} + \boldsymbol{N}_{\delta\boldsymbol{x}}\delta\boldsymbol{x} + \boldsymbol{G}(t)\boldsymbol{w}(t) + \boldsymbol{D}(t) \\ &= \boldsymbol{N}_{\delta\boldsymbol{x}}\boldsymbol{x}(t) + \boldsymbol{G}(t)\boldsymbol{w}(t) + \boldsymbol{R}(t)\end{aligned} \tag{2.22}$$

where

$$\boldsymbol{R}(t) = \hat{\boldsymbol{f}} - \boldsymbol{N}_{\delta\boldsymbol{x}}\bar{\boldsymbol{x}}(t) + \boldsymbol{D}(t) \tag{2.23}$$

where both $\boldsymbol{N}_{\delta\boldsymbol{x}}$ and $\hat{\boldsymbol{f}}$ do not contain $\boldsymbol{x}(t)$, and:

$$\boldsymbol{x}(t) = \bar{\boldsymbol{x}}(t) + \delta\boldsymbol{x}(t) \tag{2.24}$$

$$\bar{\boldsymbol{x}}(t) = E\{\boldsymbol{x}(t)\} \tag{2.25}$$

$$\boldsymbol{P}(t) = E\left\{\delta\boldsymbol{x}(t)\delta\boldsymbol{x}^{\mathrm{T}}(t)\right\} \tag{2.26}$$

According to covariance analysis theory for linear system, the propagation equations of mean vector $\bar{\boldsymbol{x}}(t)$ and covariance matrix $\boldsymbol{P}(t)$ of the random state vector $\boldsymbol{x}(t)$ under the disturbance of which noise is shown as follows:

$$\begin{cases}\dot{\bar{\boldsymbol{x}}}(t) = \hat{\boldsymbol{f}}(t) + \boldsymbol{G}(t)\bar{\boldsymbol{w}}(t) + \boldsymbol{D}(t) \\ \dot{\boldsymbol{P}}(t) = \boldsymbol{N}_{\delta\boldsymbol{x}}(t)\boldsymbol{P}(t) + \boldsymbol{P}(t)\boldsymbol{N}_{\delta\boldsymbol{x}}^{\mathrm{T}}(t) + \boldsymbol{G}(t)\boldsymbol{Q}(t)\boldsymbol{G}^{\mathrm{T}}(t)\end{cases} \tag{2.27}$$

In general, $\hat{\boldsymbol{f}}(t)$ and $\boldsymbol{N}_{\delta\boldsymbol{x}}$ contain the mean value $\bar{\boldsymbol{x}}(t)$ and covariance $\boldsymbol{P}(t)$ of $\boldsymbol{x}(t)$, the propagation equations above are nonlinear equations.

2.3.3 Gaussian Distribution-Based Describing Function

Most of the common random state vectors are subject to Gaussian distribution, so the state of a space object can also be regarded to be subject to Gaussian distribution. In this section, we firstly obtain the statistic linear describing function of nonlinear system when random variable $\boldsymbol{x}(t)$ is subject to joint Gaussian distribution. Then, apply the result to the orbital dynamic equation to analyze the propagation situation of the estimated mean and estimated covariance in high-precision orbital prediction.

According to the definition of describing function, in order to work out the describing function, we have to acquire the probability density function of $\boldsymbol{x}(t)$. In general, the analytic representations are complicate and even impossible to be obtained. If $\boldsymbol{x}(t)$ is subject to joint Gaussian distribution, the probability density function will be:

$$p(\boldsymbol{x}) = \frac{1}{\sqrt{(2\pi)^n |\boldsymbol{P}|}} \exp\left(-\frac{1}{2}\delta\boldsymbol{x}^{\mathrm{T}}\boldsymbol{P}^{-1}\delta\boldsymbol{x}\right) \tag{2.28}$$

The describing function calculation can be simplified as follows:

$$\begin{aligned} \hat{\boldsymbol{f}} &= E\{\boldsymbol{f}(\boldsymbol{x},t)\} = \int_{-\infty}^{\infty} \boldsymbol{f}(\boldsymbol{x},t)p(\boldsymbol{x})\mathrm{d}\boldsymbol{x} \\ \boldsymbol{N}_{\delta\boldsymbol{x}} &= \frac{\mathrm{d}\hat{\boldsymbol{f}}}{\mathrm{d}\bar{\boldsymbol{x}}} \end{aligned} \tag{2.29}$$

namely:

$$\hat{\boldsymbol{f}}(t) = \frac{1}{\sqrt{(2\pi)^n |\boldsymbol{P}|}} \int_{-\infty}^{\infty} \cdots \int_{-\infty}^{\infty} \boldsymbol{f}(\boldsymbol{x},t) \exp\left(-\frac{1}{2}\delta\boldsymbol{x}^{T}\boldsymbol{P}^{-1}\delta\boldsymbol{x}\right)\mathrm{d}x_1 \cdots \mathrm{d}x_n \tag{2.30}$$

$$\begin{aligned} \frac{\mathrm{d}\hat{\boldsymbol{f}}}{\mathrm{d}\bar{\boldsymbol{x}}} &\simeq \left(\frac{\partial\hat{\boldsymbol{f}}}{\partial\bar{x}_1} \quad \cdots \quad \frac{\partial\hat{\boldsymbol{f}}}{\partial\bar{x}_n}\right)^{\mathrm{T}} \\ &= \frac{1}{\sqrt{(2\pi)^n |\boldsymbol{P}|}} \int_{-\infty}^{\infty} \cdots \int_{-\infty}^{\infty} \boldsymbol{f}(\boldsymbol{x},t) \exp\left(-\frac{1}{2}\delta\boldsymbol{x}^{\mathrm{T}}\boldsymbol{P}^{-1}\delta\boldsymbol{x}\right)\delta\boldsymbol{x}^{\mathrm{T}}\mathrm{d}x_1 \cdots \mathrm{d}x_n\boldsymbol{P}^{-1} \\ &= E\left\{\boldsymbol{f}(\boldsymbol{x},t)\delta\boldsymbol{x}^{\mathrm{T}}\right\}\boldsymbol{P}^{-1} \end{aligned} \tag{2.31}$$

According to the definition of the dynamic matrix describing function of the quasi-linear system, we can learn that:

$$\boldsymbol{N}_{\delta x} = \frac{\mathrm{d}\hat{\boldsymbol{f}}}{\mathrm{d}\bar{\boldsymbol{x}}} \tag{2.32}$$

Now, the concrete solution to describing functions is presented. Set the statistic linear describing function of state equation $\boldsymbol{f} = (f_1, \ldots, f_n)^{\mathrm{T}}$ as $\hat{\boldsymbol{f}} = \left(\hat{f}_1, \ldots, \hat{f}_n\right)^{\mathrm{T}}$. If the continuous function vector $\boldsymbol{f}(\boldsymbol{x})$ of the random variable has no sine/cosine function, the Taylor expansion at mean value $\bar{\boldsymbol{x}}$ shall be presented as follows: (the case with sine/cosine functions shall be subject to special treatment, refer to literature [6])

$$\boldsymbol{f}(\boldsymbol{x}) = \boldsymbol{f}(\bar{\boldsymbol{x}} + \delta\boldsymbol{x}) = \boldsymbol{f}(\bar{\boldsymbol{x}}) + \boldsymbol{D}_{\delta x}\boldsymbol{f} + \frac{1}{2}\boldsymbol{D}_{\delta x}^2\boldsymbol{f} + \boldsymbol{R}_2(\boldsymbol{x}) \tag{2.33}$$

where $\boldsymbol{R}_2(\boldsymbol{x})$ is the remainder of Taylor Formula in second order; $\boldsymbol{D}_{\delta x}\boldsymbol{f}$ is the total differential of $\boldsymbol{f}(\cdot)$ disturbed at $\bar{\boldsymbol{x}}$ caused by disturbance $\delta\boldsymbol{x}$. The equations in the first order and second order shall be presented respectively as follows:

$$\begin{cases} \boldsymbol{D}_{\delta x}\boldsymbol{f} = \sum\limits_{p=1}^{n} \left(x_p - \bar{x}_p\right) \frac{\partial}{\partial x_p} \boldsymbol{f}(\boldsymbol{x}) \Big|_{\boldsymbol{x}=\bar{\boldsymbol{x}}} \\ \boldsymbol{D}_{\delta x}^2\boldsymbol{f} = \sum\limits_{p=1}^{n}\sum\limits_{q=1}^{n} \left(x_p - \bar{x}_p\right)\left(x_q - \bar{x}_q\right) \frac{\partial^2}{\partial x_p \partial x_q} \boldsymbol{f}(\boldsymbol{x}) \Big|_{\boldsymbol{x}=\bar{\boldsymbol{x}}} \end{cases} \tag{2.34}$$

Ignoring $\boldsymbol{R}_2(\boldsymbol{x})$ and doing the expectation of Eq. (2.33), the function vector $\boldsymbol{f}(\boldsymbol{x})$ can be linearized as follows:

$$E\{\boldsymbol{f}(\boldsymbol{x})\} = E\{\boldsymbol{f}(\bar{\boldsymbol{x}})\} + E\{\boldsymbol{D}_{\delta x}\boldsymbol{f}\} + \frac{1}{2}E\{\boldsymbol{D}_{\delta x}^2\boldsymbol{f}\} \tag{2.35}$$

The scalar form is

$$\begin{aligned} E\{\boldsymbol{f}(\boldsymbol{x})\} = E\{\boldsymbol{f}(\bar{\boldsymbol{x}})\} &+ E\left\{\sum_{p=1}^{n} \left(x_p - \bar{x}_p\right) \frac{\partial}{\partial x_p} \boldsymbol{f}(\boldsymbol{x}) \Big|_{\boldsymbol{x}=\bar{\boldsymbol{x}}}\right\} \\ &+ \frac{1}{2}E\left\{\sum_{p=1}^{n}\sum_{q=1}^{n} \left(x_p - \bar{x}_p\right)\left(x_q - \bar{x}_q\right) \frac{\partial^2}{\partial x_p \partial x_q} \boldsymbol{f}(\boldsymbol{x}) \Big|_{\boldsymbol{x}=\bar{\boldsymbol{x}}}\right\} \end{aligned} \tag{2.36}$$

It can be noticed that:

$$E\{\boldsymbol{D}_{\delta x}\boldsymbol{f}\} = E\left\{\sum_{p=1}^{n} \left(x_p - \bar{x}_p\right) \frac{\partial}{\partial x_p} \boldsymbol{f}(\boldsymbol{x}) \Big|_{\boldsymbol{x}=\bar{\boldsymbol{x}}}\right\} = 0 \tag{2.37}$$

Then,

$$E\{\boldsymbol{f}(\boldsymbol{x})\} = \boldsymbol{f}(\bar{\boldsymbol{x}}) + \frac{1}{2}E\left\{\sum_{p=1}^{n}\sum_{q=1}^{n}\left(x_p - \bar{x}_p\right)\left(x_q - \bar{x}_q\right)\frac{\partial^2}{\partial x_p \partial x_q}\boldsymbol{f}(\boldsymbol{x})\Big|_{\boldsymbol{x}=\bar{\boldsymbol{x}}}\right\} \tag{2.38}$$

According to the statistic theory, the statistic linear describing function of $\boldsymbol{f}(\boldsymbol{x})$ is:

$$\hat{\boldsymbol{f}}(\boldsymbol{x}) = E\{\boldsymbol{f}(\boldsymbol{x})\} = \boldsymbol{f}(\bar{\boldsymbol{x}}) + \frac{1}{2}E\left\{\sum_{p=1}^{n}\sum_{q=1}^{n}\left(x_p - \bar{x}_p\right)\left(x_q - \bar{x}_q\right)\frac{\partial^2}{\partial x_p \partial x_q}\boldsymbol{f}(\boldsymbol{x})\Big|_{\boldsymbol{x}=\bar{\boldsymbol{x}}}\right\} \tag{2.39}$$

Where the ith factor of $\hat{\boldsymbol{f}}(\boldsymbol{x})$ shall be:

$$\hat{f}_i(\boldsymbol{x}) = f_i(\bar{\boldsymbol{x}}) + \frac{1}{2}E\left\{\sum_{p=1}^{n}\sum_{q=1}^{n}\left(x_p - \bar{x}_p\right)\left(x_q - \bar{x}_q\right)\frac{\partial^2}{\partial x_p \partial x_q}f_i(\boldsymbol{x})\Big|_{\boldsymbol{x}=\bar{\boldsymbol{x}}}\right\} \tag{2.40}$$

Covariance matrix of vector $\boldsymbol{x}$ about the mean value $\bar{\boldsymbol{x}}$ shall be:

$$\begin{aligned}\boldsymbol{P} &= E\left\{\delta\boldsymbol{x}\delta\boldsymbol{x}^{\mathrm{T}}\right\} = E\left\{(\boldsymbol{x}-\bar{\boldsymbol{x}})(\boldsymbol{x}-\bar{\boldsymbol{x}})^{\mathrm{T}}\right\} \\ &= \begin{pmatrix} E\left\{(x_1-\bar{x}_1)^2\right\} & \cdots & E\{(x_1-\bar{x}_1)(x_n-\bar{x}_n)\} \\ \vdots & & \vdots \\ E\{(x_n-\bar{x}_n)(x_1-\bar{x}_1)\} & \cdots & E\left\{(x_n-\bar{x}_n)^2\right\} \end{pmatrix} \triangleq \begin{pmatrix} P_{11} & \cdots & P_{1n} \\ \vdots & & \vdots \\ P_{n1} & \cdots & P_{nn} \end{pmatrix}\end{aligned} \tag{2.41}$$

Then, Eqs. (2.39) and (2.40) can be presented as follows:

$$\hat{\boldsymbol{f}}(\boldsymbol{x}) = \boldsymbol{f}(\bar{\boldsymbol{x}}) + \frac{1}{2}\sum_{p=1}^{n}\sum_{q=1}^{n}P_{pq}\frac{\partial^2}{\partial x_p \partial x_q}\boldsymbol{f}(\boldsymbol{x})\Big|_{\boldsymbol{x}=\bar{\boldsymbol{x}}} \tag{2.42}$$

$$\hat{f}_i(\boldsymbol{x}) = f_i(\bar{\boldsymbol{x}}) + \frac{1}{2}\sum_{p=1}^{n}\sum_{q=1}^{n}P_{pq}\frac{\partial^2}{\partial x_p \partial x_q}f_i(\boldsymbol{x})\Big|_{\boldsymbol{x}=\bar{\boldsymbol{x}}} \tag{2.43}$$

At this moment,

$$\boldsymbol{N}_{\delta\boldsymbol{x}} = \frac{\mathrm{d}\hat{\boldsymbol{f}}}{\mathrm{d}\bar{\boldsymbol{x}}} = \frac{\mathrm{d}\boldsymbol{f}(\bar{\boldsymbol{x}})}{\mathrm{d}\bar{\boldsymbol{x}}} + \frac{\mathrm{d}}{\mathrm{d}\bar{\boldsymbol{x}}}\left(\frac{1}{2}\sum_{p=1}^{n}\sum_{q=1}^{n}P_{pq}\frac{\partial^2}{\partial x_p \partial x_q}f_i(\boldsymbol{x})\Big|_{\boldsymbol{x}=\bar{\boldsymbol{x}}}\right) \tag{2.44}$$

Comparing with linear system, Eq. (2.44) derived from the quasi-linear system has a second-order corrective term. Therefore, the description on covariance propagation is much more accurate than the Ricatti Formula for nonlinear system.

If the signal and information systems concerned are nonlinear systems, and the optimal estimation is not limited to be a linear one, or the noise is in non-Gaussian distribution, it will be relatively difficult to present the covariance matrix. The martingale representation of nonlinear system error covariance matrix is presented in literature [18]. When doing covariance analysis, high-order statistics approaching method shall be adopted.

Providing that the initial state error is Gaussian white noise, a comparison had been made upon the covariance matrixes which were worked out through CADET and Monte Carlos Method. The comparison in literature [19] presents the same result which has a relatively higher calculating precision.

In addition, literature [20] provides a reliable research on the non-Gaussian error propagation of orbit and substitutes the Gaussian Confidence Ellipsoid with the maximum boundary calibrated error range of undetermined forecasting cloud.

2.3.4 CADET's Application on Orbit

Space object dynamic differential equation can be presented as:

$$\dot{\boldsymbol{x}}(t) = f(\boldsymbol{x}(t), t) + \boldsymbol{w}(t), \quad \boldsymbol{w}(t) \sim N(0, \boldsymbol{Q}(t)) \tag{2.45}$$

Providing that the system noise $\boldsymbol{w}(t)$ is white noise with an expectation value of 0, the spectrum density matrix is $\boldsymbol{Q}(t)$. And the orbital state estimated mean value and covariance at initial time shall be:

$$\boldsymbol{x}(0) \sim N(\bar{\boldsymbol{x}}_0, \quad \boldsymbol{P}_0) \tag{2.46}$$

According to the covariance describing function method, orbital propagation is to integrate the following propagation equations of estimated mean value and covariance:

$$\dot{\bar{\boldsymbol{x}}}(t) = \hat{\boldsymbol{f}}(\bar{\boldsymbol{x}}(t), t) + \bar{\boldsymbol{w}}(t) \tag{2.47}$$

$$\hat{\boldsymbol{f}}(\bar{\boldsymbol{x}}(t), t) = \boldsymbol{f}(\bar{\boldsymbol{x}}(t), t) + \frac{1}{2}\sum_{p=1}^{n}\sum_{q=1}^{n} P_{pq}\frac{\partial^2}{\partial x_p \partial x_q}\boldsymbol{f}(\boldsymbol{x}(t), t)\Big|_{\boldsymbol{x}=\bar{\boldsymbol{x}}} \tag{2.48}$$

$$\dot{\boldsymbol{P}}(t) = \boldsymbol{F}(\bar{\boldsymbol{x}}(t), t)\boldsymbol{P}(t) + \boldsymbol{P}(t)\boldsymbol{F}^{\mathrm{T}}(\bar{\boldsymbol{x}}(t), t) + \boldsymbol{Q}(t) \tag{2.49}$$

$$\boldsymbol{F}(\bar{\boldsymbol{x}}(t), t) = \frac{\partial \hat{\boldsymbol{f}}(\bar{\boldsymbol{x}}(t), \quad t)}{\partial \bar{\boldsymbol{x}}(t)} \tag{2.50}$$

Providing that the mean value of state vector $\boldsymbol{x}$ is $\bar{\boldsymbol{x}} = (\bar{\boldsymbol{r}}^{\mathrm{T}}, \bar{\boldsymbol{v}}^{\mathrm{T}})^{\mathrm{T}}$, the differential equation of mean value shall be $\dot{\bar{\boldsymbol{x}}} = (\bar{\boldsymbol{v}}^{\mathrm{T}}, \bar{\boldsymbol{a}}^{\mathrm{T}})^{\mathrm{T}}$. If the geocentric distance is 7000 km, the second-order partial derivative of the acceleration of gravity with respect to the radius vector is with the magnitude of $\mathrm{d}^2(\mu/r^2)/\mathrm{d}r^2 \approx 10^{-12}$.

If the position variance is with a magnitude of 10^6 m^2, the magnitude of the second-order term of Taylor expansion is about 10^{-6}, which is equal to the magnitude of the non-spherical perturbation term J_4. In general calculation, only the J_2 impact of the compression of the Earth is considered in the second-order partial derivative. If the orbital altitude is relatively low, the second-order partial derivative of atmospheric damping shall also be taken into account.

Integral of mean value and covariance shall be conducted in ECI coordinate system and error analysis shall be conducted in RSW coordinate system as follows:

$$\boldsymbol{P}_{\mathrm{RSW}} = \boldsymbol{J}\boldsymbol{P}_{\mathrm{ECI}}\boldsymbol{J}^{\mathrm{T}} \tag{2.51}$$

$$\boldsymbol{J} = \begin{pmatrix} \boldsymbol{M}^{\mathrm{T}}_{\mathrm{RSW}\to\mathrm{ECI}} & 0 \\ 0 & \boldsymbol{M}^{\mathrm{T}}_{\mathrm{RSW}\to\mathrm{ECI}} \end{pmatrix} = \begin{pmatrix} \begin{pmatrix} \hat{\boldsymbol{R}} & \hat{\boldsymbol{S}} & \hat{\boldsymbol{W}} \end{pmatrix}^{\mathrm{T}} & 0 \\ 0 & \begin{pmatrix} \hat{\boldsymbol{R}} & \hat{\boldsymbol{S}} & \hat{\boldsymbol{W}} \end{pmatrix}^{\mathrm{T}} \end{pmatrix} \tag{2.52}$$

According to the space object dynamics equation mentioned in last section, we can analysis the initial mean value and error propagation situation in this section. Ignoring the impact of noise and considering the impact of major second-order partial derivatives, at this moment the mean value differential equation will be the same as Eq. (2.47) and the covariance propagation equation is:

$$\dot{\boldsymbol{P}}(t) = \boldsymbol{F}(\bar{\boldsymbol{x}}(t), t)\boldsymbol{P}(t) + \boldsymbol{P}(t)\boldsymbol{F}^{\mathrm{T}}(\bar{\boldsymbol{x}}(t), t) \tag{2.53}$$

The initial condition is

$$\boldsymbol{x}(0) \sim N(\bar{\boldsymbol{x}}_0, \boldsymbol{P}_0) \tag{2.54}$$

Select four typical space objects including the Sun Synchronous Orbit (SSO), the MEO, the Highly Eccentric Orbit (HEO), and the GEO. Refer to Table 2.1 for the types of objects and orbits. Refer to Table 2.2 for the orbital elements of objects (epoch times are UTC 00:00:00, August 1st 2008).

Table 2.1 Types of objects and orbits

S/N	Type of orbit	Type of object	Object name	Object code
①	SSO	Earth Resources Satellite	ERS-2	23560
②	MEO	GPS Satellite	GPSBlockHa	25030
③	HEO	Molnyia Satellite	Molnyia3-35	20052
④	GEO	Galaxy Communication Satellite	Galaxy-11	26038

Table 2.2 Orbital elements of objects

S/N	*a*/km	*e*	*i*/(°)	Ω/(°)	ω/(°)	*M*/(°)
①	7151.800091	0.0000917	98.5690	76.5485	99.0473	261.0823
②	26558.682691	0.010179	56.277	62.334	163.339	273.257
③	25663.740026	0.740361	63.463	359.792	270.021	40.168
④	42166.577215	0.000036	0.068	109.622	217.823	41.434

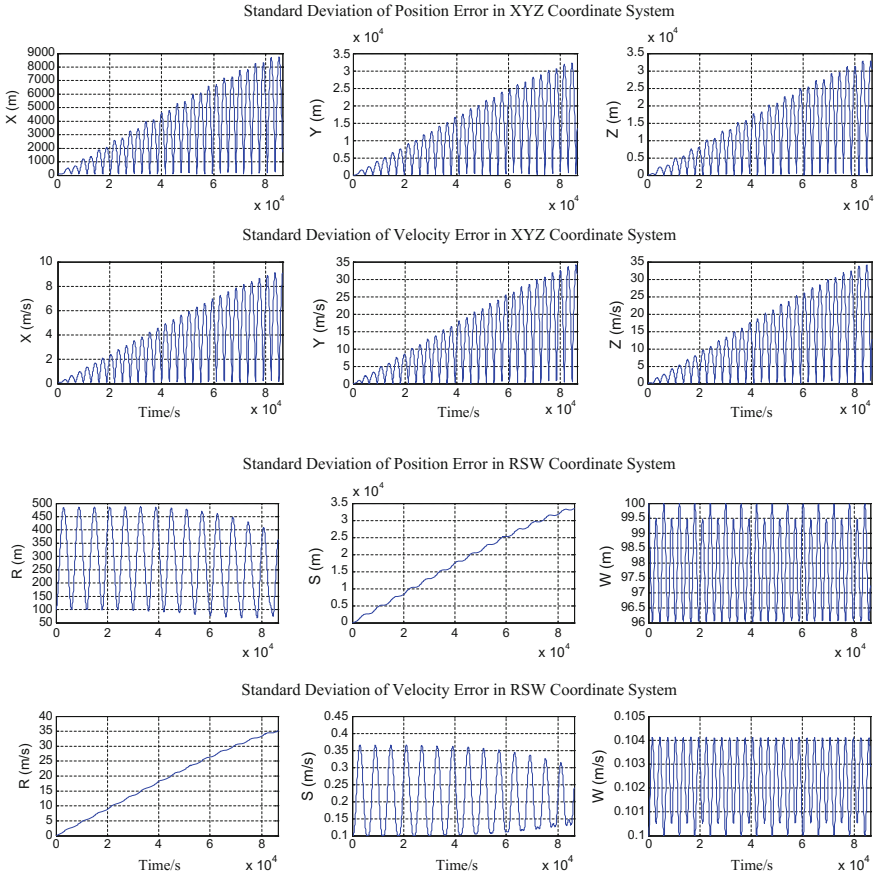

Fig. 2.5 Error propagation curve of object ①

Ignoring the model noise and providing that the standard deviations of the position error in each axis direction at initial state is 100 m and that of the velocity error is 0.1 m, the error divergence situations in XYZ and RSW coordination systems in the next day are shown as Figs. 2.5 2.6, 2.7, 2.8 and 2.9.

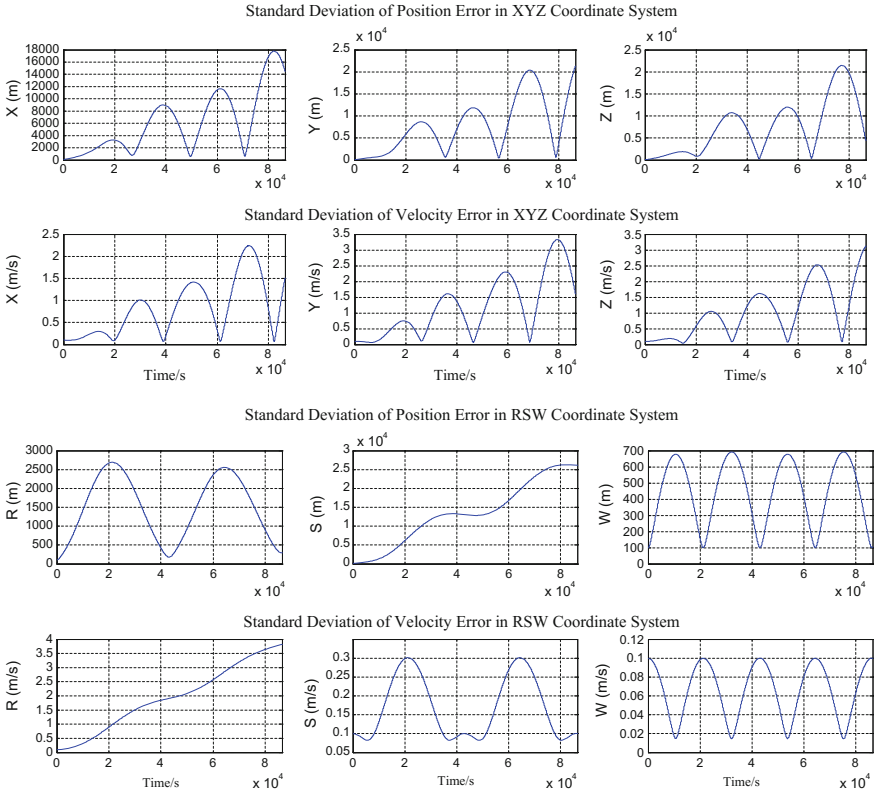

Fig. 2.6 Error propagation curve of object ②

As shown in Figs. 2.5, 2.6, 2.7, 2.8 and 2.9, both the radial position and velocity errors of Object ① present relatively high levels of divergence, and the standard deviation reached 35 km in the next day due to its relatively low orbital altitude and large influence of atmospheric damping.

Object ② presents a relatively mild degree of error divergence due to its relatively high orbital altitude and relatively small influence of atmospheric damping. In the next day, its standard deviations of position and velocity errors reached 27 km and 3.7 m/s, respectively.

As Object ③ is in an elliptic orbit, it is subject to the most complicated perturbation factors and the most serious error divergence situation. In the next day, its standard deviations of position and velocity errors reached 70 km and 60 m/s respectively. Due to the relatively large orbital eccentricity and flight-path angle, a relatively obvious difference in RSW and NTW coordinate systems has been found.

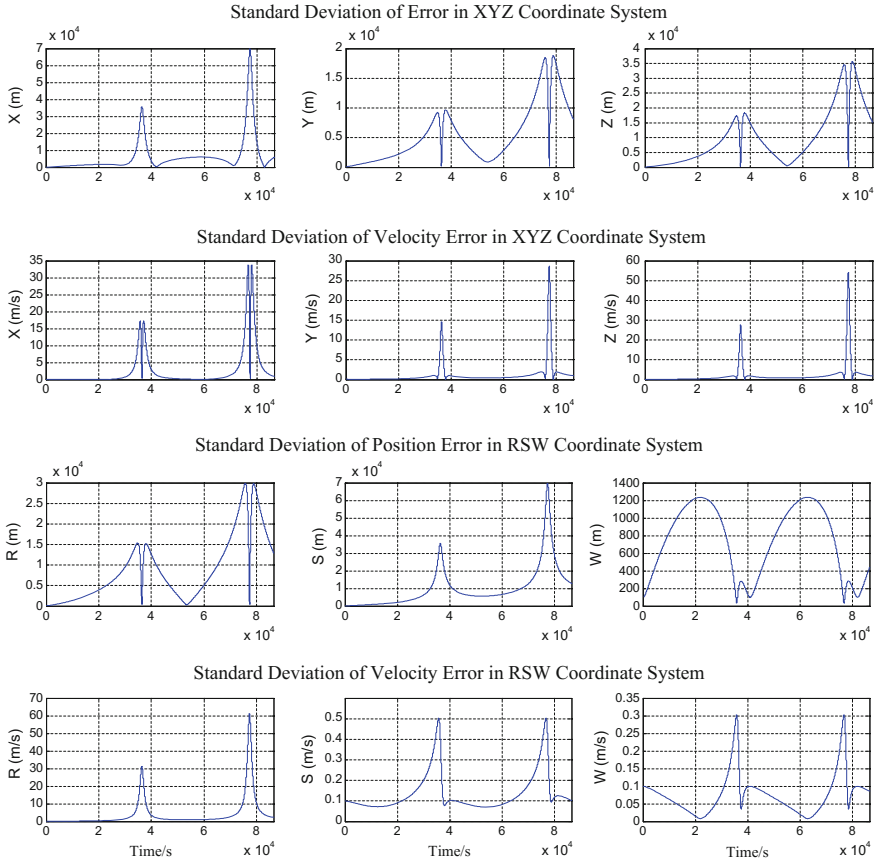

Fig. 2.7 Error propagation curve of object ③

The propagation curve of error standard deviation in NTW coordinate system had also been drawn. As can be seen in Fig. 2.10, NTW coordinate system is more applicable to elliptic orbits than RSW coordinate system.

Object ④ is with the highest orbital altitude and the smallest influence of atmospheric damping. Therefore it has the minimum error divergence in radial velocity, whose standard deviation only reached 2 m/s in the next day. However, it has a relatively serious error divergence in position, whose standard deviation reached 27 km in the next day.

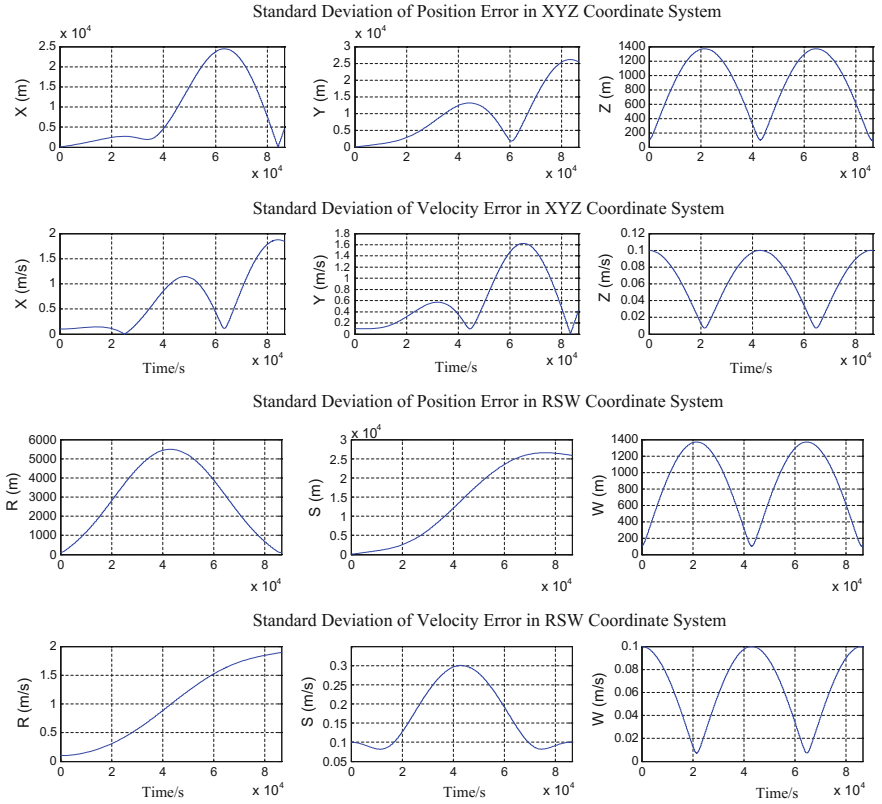

Fig. 2.8 Error propagation curve of object ④ (one day later)

2.4 Orbital Error Analysis Based on Relative Motion Theory

Relative motion of spacecraft refers to the motion of one or one set of spacecrafts relative to a target spacecraft or a virtual spacecraft under the action of the same gravitational field [21]. In contrast with its absolute motion (classical orbital motion), the relative motion of a spacecraft discusses questions in more variable forms and influenced by more complicated factors. Modeling and analysis of the relative motion of spacecraft had already gone through in-depth studies by various forms of models, which have been successfully applied to space missions including space rendezvous and docking, spacecraft in-orbit services, spacecraft formation flying, space-based space object surveillance, short distance observation, space robot capture, and so on [21].

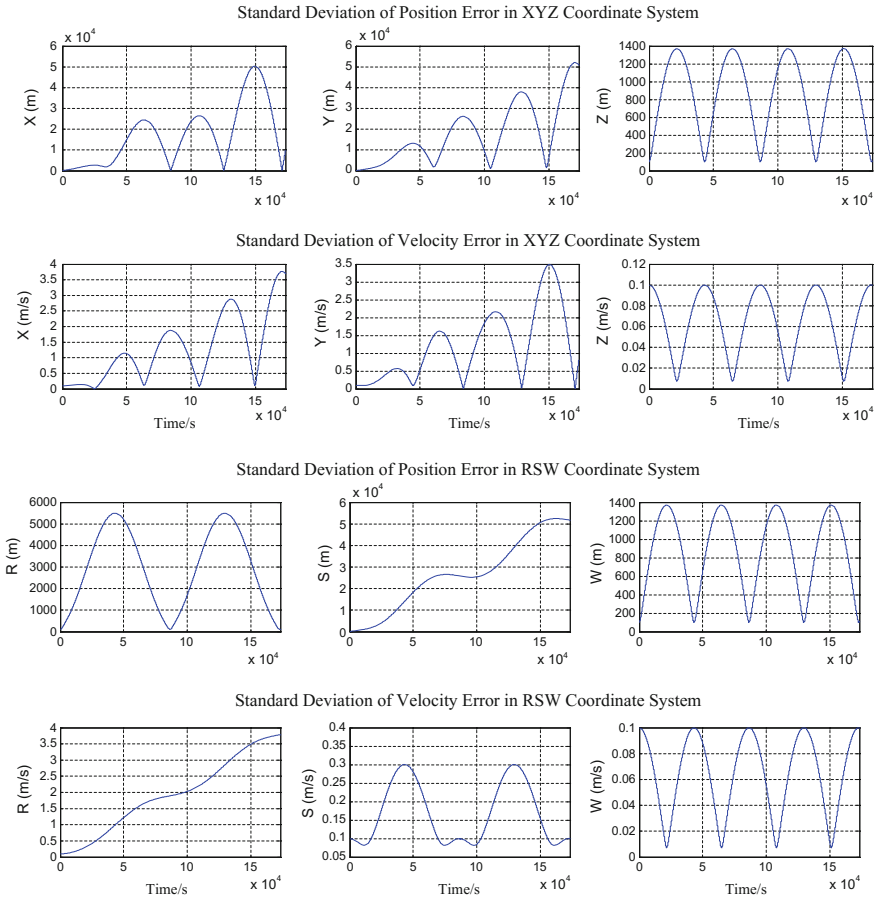

Fig. 2.9 Error propagation curve of object ④ (two days later)

Error (less than dozens of kilometers) of space object orbit propagation is a smaller value comparing to its radius vector (generally no less than 6500 km). Thus, the true and predict states of a space object can be considered as two objects with a short distance: a real and a virtual one, orbit prediction errors as relative motion between these two objects, then the relative motion theory in short distance can be used to study the characteristics of orbit prediction errors.

In this section, we firstly do initial error propagation analysis on circular and elliptical orbits using C-W and T-H equations based on algebraic models for relative motion. Then we make correlation characterization analysis on position and velocity prediction errors of nearly circular orbit using geometrical models for relative motion and then discuss its application in initial error selection.

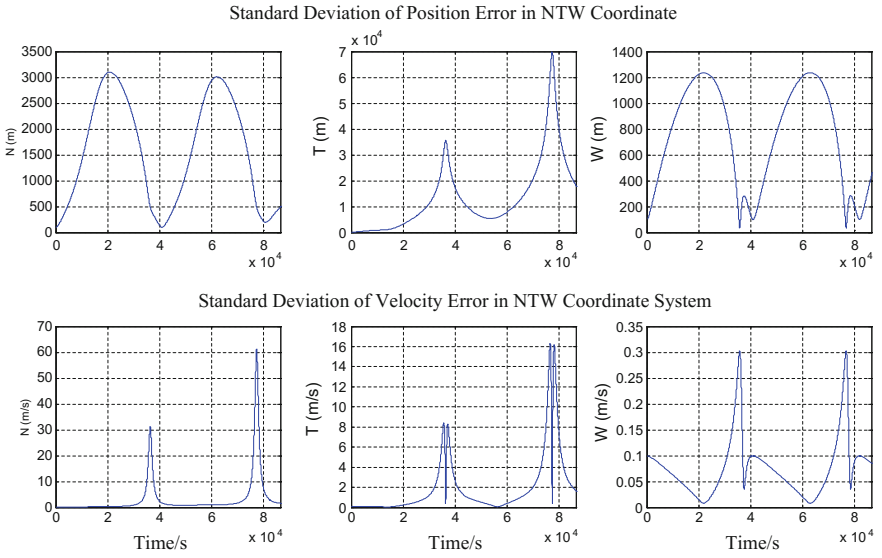

Fig. 2.10 Error propagation curve of object ③ in NTW coordinate system

2.4.1 Initial Error Propagation Based on Algebraic Models

Orbit prediction errors of space objects consist of initial and model errors. Initial error in orbit prediction propagates with time. Its propagation characteristics and tendencies differ with the type of orbits. Decoupling analysis on initial and model errors of orbit prediction is often used to simplify the problem. For initial error analysis, orbit prediction models are considered to be accurate without any model errors, which indicate that the difference of perturbation forces between prediction models and actual orbits is considered to be zero. Thus we can get the propagation characteristics of initial errors.

Generally, studies on relative motion neglect attitude motions. There are two types of models [22–26]. One is algebraic method, also known as the dynamic method, which is based on relative dynamic equation and easy for the guidance and control of relative motion. Another is geometrical method, also known as the kinematic method, which is based on models of relative motion expressed by orbital elements and easy for orbital design and perturbation analysis. The algebraic method is based on the basic dynamic equations described by absolute position vectors of two spacecraft and builds a relative motion model in relative motion coordinate system by assumptions and simplifications. The model is expressed in differential equation sets, and makes predictions for the relative motion state if initial conditions are known, so that it is applicable for analyzing the propagation characterization of initial errors of the orbit prediction.

1. Algebraic models for relative motion

The application of relative motion theory in analysis of orbit prediction errors of space object is discussed in this section. One of the two space objects is the dominant object and the other is the subordinate object, corresponding to the target spacecraft and the tracing spacecraft in space rendezvous and docking.

The algebraic models for relative motion has been developed by Hill [27] and Clohessy and Wiltshire [28]. Vallado [2] has presented the development as well. We build relative motion models based on algebraic method, starting from the basic motion equations described by absolute position vectors of the two objects and establish the relative motion model in the *RSW* coordinate system of the dominating object. If we take $\boldsymbol{r}_\mathrm{p}$ and $\boldsymbol{r}_\mathrm{s}$ as the respective absolute position vectors of the dominating and subordinate objects in *ECI* coordinate system, the orbital dynamic equations of the dominating and subordinate objects in ECI coordinate system are as follows

$$\ddot{\boldsymbol{r}}_\mathrm{p} = -\frac{\mu}{r_\mathrm{p}^3}\boldsymbol{r}_\mathrm{p} + \boldsymbol{f}_\mathrm{p}, \quad \ddot{\boldsymbol{r}}_\mathrm{s} = -\frac{\mu}{r_\mathrm{s}^3}\boldsymbol{r}_\mathrm{s} + \boldsymbol{f}_\mathrm{s} \tag{2.55}$$

where μ is constant of earth gravitation; $\boldsymbol{f}_\mathrm{p}$ and $\boldsymbol{f}_\mathrm{s}$ are respectively perturbation accelerations generated by all perturbation forces excluding gravity of the center of the Earth acting on the dominating and subordinate objects. For error analysis, the two objects are considered to be without control forces acting on them.

Relative position vector from the dominating object to the subordinate object $\boldsymbol{r} = \boldsymbol{r}_\mathrm{s} - \boldsymbol{r}_\mathrm{p}$, from Eq. (2.55) we can get

$$\frac{\mathrm{d}^2\boldsymbol{r}}{\mathrm{d}t^2} = \ddot{\boldsymbol{r}}_\mathrm{s} - \ddot{\boldsymbol{r}}_\mathrm{p} = -\frac{\mu}{r_\mathrm{s}^3}\boldsymbol{r}_\mathrm{s} + \frac{\mu}{r_\mathrm{p}^3}\boldsymbol{r}_\mathrm{p} + \boldsymbol{f}_\mathrm{s} - \boldsymbol{f}_p = \frac{\mu}{r_\mathrm{p}^3}\left(\boldsymbol{r}_\mathrm{p} - \left(\frac{r_\mathrm{p}}{r_\mathrm{s}}\right)^3\boldsymbol{r}_\mathrm{s}\right) + \boldsymbol{f} \tag{2.56}$$

where $\boldsymbol{f} = \boldsymbol{f}_\mathrm{s} - \boldsymbol{f}_\mathrm{p}$ is the difference of the perturbation accelerations acting on the two objects.

Equation (2.56) is the expression of relative dynamic equation in ECI coordinate system, which is an accurate equation of relative motion without any simplification.

Build a relative dynamic equation in RSW coordinate system of the dominating object. The relation of the absolute derivative and relative derivative is as follows:

$$\frac{\mathrm{d}^2\boldsymbol{r}}{\mathrm{d}t^2} = \frac{\delta^2\boldsymbol{r}}{\delta t^2} + 2\boldsymbol{\omega}_\mathrm{p} \times \frac{\delta\boldsymbol{r}}{\delta t} + \boldsymbol{\omega}_\mathrm{p} \times \left(\boldsymbol{\omega}_\mathrm{p} \times \boldsymbol{r}\right) + \dot{\boldsymbol{\omega}}_\mathrm{p} \times \boldsymbol{r} \tag{2.57}$$

where $\delta^2\boldsymbol{r}/\delta t^2$ and $\delta\boldsymbol{r}/\delta t$ are the relative acceleration vector and elative velocity vector of the subordinate object in *RSW* coordinate system of the dominating object, respectively; $\dot{\boldsymbol{\omega}}_\mathrm{p}$ and $\boldsymbol{\omega}_\mathrm{p}$ are the angular acceleration vector and angular velocity vector of the dominating object, respectively.

From Eqs. (2.56) and (2.57) we can get

$$\frac{\delta^2 \boldsymbol{r}}{\delta t^2} + 2\boldsymbol{\omega}_\mathrm{p} \times \frac{\delta \boldsymbol{r}}{\delta t} + \boldsymbol{\omega}_\mathrm{p} \times \left(\boldsymbol{\omega}_\mathrm{p} \times \boldsymbol{r}\right) + \dot{\boldsymbol{\omega}}_\mathrm{p} \times \boldsymbol{r} = \frac{\mu}{r_\mathrm{p}^3}\left(\boldsymbol{r}_\mathrm{p} - \left(\frac{r_\mathrm{p}}{r_\mathrm{s}}\right)^3 \boldsymbol{r}_\mathrm{s}\right) + \boldsymbol{f} \tag{2.58}$$

In *RSW* coordinate system of the dominating object, assume the relative position vector to be $\boldsymbol{r} = (x \quad y \quad z)^\mathrm{T}_{RSW}$, we can get

$$\begin{aligned} &\tfrac{\delta \boldsymbol{r}}{\delta t} = (\dot{x} \quad \dot{y} \quad \dot{z})^\mathrm{T}, \quad \tfrac{\delta^2 \boldsymbol{r}}{\delta t^2} = (\ddot{x} \quad \ddot{y} \quad \ddot{z})^\mathrm{T} \\ &\boldsymbol{\omega}_\mathrm{p} = \left(0 \quad 0 \quad \dot{\theta}\right)^\mathrm{T}, \quad \dot{\boldsymbol{\omega}}_\mathrm{p} = \left(0 \quad 0 \quad \ddot{\theta}\right)^\mathrm{T} \\ &\boldsymbol{r}_\mathrm{p} = (r_\mathrm{p} \quad 0 \quad 0)^\mathrm{T}, \quad \boldsymbol{r}_\mathrm{s} = (r_\mathrm{p} + x \quad y \quad z)^\mathrm{T} \end{aligned} \tag{2.59}$$

where θ is the true anomaly of the dominating object orbit.

Substitute Eq. (2.59) into Eq. (2.58) yields

$$\begin{cases} \ddot{x} = 2\dot{y}\dot{\theta} + x\dot{\theta}^2 + y\ddot{\theta} + \frac{\mu}{r_\mathrm{p}^2} - \frac{\mu}{r_\mathrm{s}^3}\left(r_\mathrm{p} + x\right) + f_x \\ \ddot{y} = -2\dot{x}\dot{\theta} + y\dot{\theta}^2 - x\ddot{\theta} - \frac{\mu}{r_\mathrm{s}^3} y + f_y \\ \ddot{z} = -\frac{\mu}{r_\mathrm{s}^3} z + f_z \end{cases} \tag{2.60}$$

Equation (2.60) is the expression of relative dynamic equation in *RSW* coordinate system, which is an accurate equation of relative motion without any simplification.

Geocentric distance of the subordinate object can be expressed with geocentric distance of the dominating object r_p and the relative position vector $\boldsymbol{r}$

$$r_s = \left[\left(r_\mathrm{p} + x\right)^2 + y^2 + z^2\right]^{\frac{1}{2}} = \left(r_\mathrm{p}^2 + 2r_\mathrm{p}x + r^2\right)^{\frac{1}{2}} = r_\mathrm{p}\left(1 + 2\frac{x}{r_\mathrm{p}} + \frac{r^2}{r_\mathrm{p}^2}\right)^{\frac{1}{2}} \tag{2.61}$$

Suppose that the distance between the dominating and subordinate objects is far less than their geocentric distance ($r \ll r_\mathrm{p}$), Eq. (2.61) can be written as

$$\frac{1}{r_\mathrm{s}^3} = \frac{1}{r_\mathrm{p}^3}\left(1 + 2\frac{x}{r_\mathrm{p}} + \frac{r^2}{r_\mathrm{p}^2}\right)^{-\frac{3}{2}} \approx \frac{1}{r_\mathrm{p}^3}\left(1 - \frac{3x}{r_\mathrm{p}}\right) \tag{2.62}$$

Substitute Eq. (2.62) into Eq. (2.60) yields

$$\begin{cases} \ddot{x} = 2\dot{y}\dot{\theta} + x\dot{\theta}^2 + y\ddot{\theta} + \frac{2\mu x}{r_\mathrm{p}^3} + \frac{3\mu x^2}{r_\mathrm{p}^4} + f_x \\ \ddot{y} = -2\dot{x}\dot{\theta} + y\dot{\theta}^2 - x\ddot{\theta} - \frac{\mu y}{r_\mathrm{p}^3} + \frac{3\mu xy}{r_\mathrm{p}^4} + f_y \\ \ddot{z} = -\frac{\mu z}{r_\mathrm{p}^3} + \frac{3\mu xz}{r_\mathrm{p}^4} + f_z \end{cases} \tag{2.63}$$

Furthermore, neglecting the quadratic term $(\mu \boldsymbol{r}/r_{\mathrm{p}}^4)$ in Eq. (2.63), we can get a linearized expression of relative motion equation

$$\begin{cases} \ddot{x} - 2\dot{\theta}\dot{y} - \dot{\theta}^2 x - \ddot{\theta} y - \frac{2\mu x}{r_{\mathrm{p}}^3} = f_x \\ \ddot{y} + 2\dot{\theta}\dot{x} + \ddot{\theta} x - \dot{\theta}^2 y + \frac{\mu y}{r_{\mathrm{p}}^3} = f_y \\ \ddot{z} + \frac{\mu z}{r_{\mathrm{p}}^3} = f_z \end{cases} \tag{2.64}$$

Deduction of Eq. (2.64) only needs to suppose that the distance between the dominating and subordinate objects is far less than their geocentric distances, no restrictions on orbital eccentricity is required, and it is applicable to all orbital shapes. From Eq. (2.64) we can tell that the relative motion along the direction W (vertical to the orbital plane) is independent whereas the relative motions along the direction R and S are coupled with each other.

(1) C-W equation

If the dominating object is in a nearly circular orbit, i.e. $e_{\mathrm{p}} \approx 0$, we have

$$\dot{\theta} \approx n, \quad \ddot{\theta} \approx 0, \quad \frac{\mu}{r_{\mathrm{p}}^3} \approx n^2 \tag{2.65}$$

where n is average angular velocity of the dominating object.

Substituting Eq. (2.65) into Eq. (2.64) and neglecting the difference of perturbation forces of the two objects, we can get

$$\begin{cases} \ddot{x} - 2n\dot{y} - 3n^2 x = 0 \\ \ddot{y} + 2n\dot{x} = 0 \\ \ddot{z} + n^2 z = 0 \end{cases} \tag{2.66}$$

Equation (2.66) is the Clohessy-Wiltshire or C-W equation, also known as Hill's equation or H-C-W equation [2].

If we mark the initial time of relative motion with subscript "0", the corresponding initial conditions is $(x_0, y_0, z_0, \dot{x}_0, \dot{y}_0, \dot{z}_0)$ and we can get the analytical solution of relative motion at any time t by integrating Eq. (2.66). The analytical solution of relative position is

$$\begin{cases} x(t) = \frac{\dot{x}_0}{n} \sin nt - \left(\frac{2\dot{y}_0}{n} + 3x_0\right) \cos nt + 2\left(\frac{\dot{y}_0}{n} + 2x_0\right) \\ y(t) = 2\left(\frac{2\dot{y}_0}{n} + 3x_0\right) \sin nt + \frac{2\dot{x}_0}{n} \cos nt - 3(\dot{y}_0 + 2nx_0)t + \left(y_0 - \frac{2\dot{x}_0}{n}\right) \\ z(t) = \frac{\dot{z}_0}{n} \sin nt + z_0 \cos nt \end{cases} \tag{2.67}$$

The analytical solution of relative velocity is

$$\begin{cases} \dot{x}(t) = (2\dot{y}_0 + 3nx_0)\sin nt + \dot{x}_0 \cos nt \\ \dot{y}(t) = -2\dot{x}_0 \sin nt + 2(2\dot{y}_0 + 3nx_0)\cos nt - 3(\dot{y}_0 + 2nx_0) \\ \dot{z}(t) = -nz_0 \sin nt + \dot{z}_0 \cos nt \end{cases} \tag{2.68}$$

C-W equation is the most classical algebraic relative dynamic model. It takes the spherical central gravitation and circular reference orbit as assumptions, excluding the influence of perturbation forces. Although bearing some errors, it provides the simplest relative motion relationship and is widely used in satellite formation flying, space rendezvous, and other fields.

(2) T-H equation

In order to eliminate the restriction of circular reference orbit, Tschauner and Hempel assumed that the object distance is a first order small value comparing to the geocentric distance. According to variable substitution, they made the true anomaly of the dominating object an independent variable, thus the equation became dimensionless. Next, they simplified the nonlinear relative dynamic differential equation set into a linear time-varying equation set and got an analytical solution described with true anomaly/eccentric anomaly. The equation is called the Tschauner-Hempel Equation. (abbr. T-H equation). T-H equation describes the relative motion of objects with any eccentricity. Yamanaka got a new state transition matrix through a series of variable substitutions [29], which helped in discussion of its consistency with C-W equations. Yue et al., deduced specific expressions of state transition matrix factors expressed by positions and velocities in three-dimensional space. Converting them from angular domain into time domain, they got state transition matrix expressing actual positions and velocities [30]. Xing et al., studied relative motion issues of satellite formation flying [31–37].

If the dominating object is in an elliptical orbit, we can get a relatively simple dynamics equation by taking true anomaly θ as an independent variable. Therefore, we can get relative dynamics equations with true anomaly θ as an independent variable by making variable substitutions to Eq. (2.64) and substituting true anomaly θ for time t as the independent variable, derivative x' with respect to true anomaly for derivative $\dot{x}$ with respect to time

$$\begin{cases} x'' - \frac{2e\sin\theta}{1+e\cos\theta}x' - 2y' - \frac{3+e\cos\theta}{1+e\cos\theta}x + \frac{2e\sin\theta}{1+e\cos\theta}y = 0 \\ y'' + 2x' - \frac{2e\sin\theta}{1+e\cos\theta}y' - \frac{2e\sin\theta}{1+e\cos\theta}x - \frac{e\cos\theta}{1+e\cos\theta}y = 0 \\ z'' - \frac{2e\sin\theta}{1+e\cos\theta}z' + \frac{1}{1+e\cos\theta}z = 0 \end{cases} \tag{2.69}$$

Yamanaka made variable substitutions to Eq. (2.69) [29], with its equations given in LVLH coordinate system, whereas equations of this section given in *RSW* coordinate system. If we make $\rho = 1 + e\cos\theta$, variable substitutions are as follows:

$$(\tilde{x} \quad \tilde{y} \quad \tilde{z})^{\mathrm{T}} = \rho(x \quad y \quad z)^{\mathrm{T}} \tag{2.70}$$

Converting T-H equations to a simpler form

$$\begin{cases} \tilde{x}'' = 3\tilde{x}/\rho + 2\tilde{y}' \\ \tilde{y}'' = -2x' \\ \tilde{z}'' = -\tilde{z} \end{cases} \tag{2.71}$$

Yamanaka, by derivation, got a state transition matrix expressed in angular domain [29]. We have deduced the expression of state transition matrix of T-H equation in the *RSW* coordinate system:

$$\begin{bmatrix} x \\ y \\ z \\ \dot{x} \\ \dot{y} \\ \dot{z} \end{bmatrix} = \boldsymbol{T}(t) \begin{bmatrix} x_0 \\ y_0 \\ z_0 \\ \dot{x}_0 \\ \dot{y}_0 \\ \dot{z}_0 \end{bmatrix}, \quad \boldsymbol{T}(t) = \begin{bmatrix} t_{11} & t_{12} & 0 & t_{14} & t_{15} & 0 \\ t_{21} & t_{22} & 0 & t_{24} & t_{25} & 0 \\ 0 & 0 & t_{33} & 0 & 0 & t_{36} \\ t_{41} & t_{42} & 0 & t_{44} & t_{45} & 0 \\ t_{51} & t_{52} & 0 & t_{54} & t_{55} & 0 \\ 0 & 0 & t_{63} & 0 & 0 & t_{66} \end{bmatrix} \tag{2.72}$$

Due to the length limitation of this section, we list specific element values of the state transition matrix $\boldsymbol{T}(t)$ in Appendix A. The only assumption that makes the state transition matrix tenable is that the relative distance is far less than the geocentric distances of space objects and hence it can be applicable to elliptical orbit with any eccentricity. When we have already known initial conditions, the matrix can be directly used to calculate the state transition of the relative motion in the time domain.

2. Error propagation of near-circular orbit based on C-W equation

(1) Error propagation formula

We first use C-W equation to analyze propagation characteristics of initial errors of nearly circular orbits. $(\dot{x}, \dot{y}, \dot{z})^{\mathrm{T}}$ in Eq. (2.68) can be seen as relative velocity errors or time derivatives of relative position errors, projection of absolute velocity errors in the orbital coordination system, which is more concerned in error analysis. From the following relation of absolute and relative velocities,

$$\frac{\mathrm{d}\boldsymbol{r}}{\mathrm{d}t} = \frac{\delta \boldsymbol{r}}{\delta t} + \boldsymbol{\omega}_{\mathrm{p}} \times \boldsymbol{r} \tag{2.73}$$

we can get

$$\Delta \boldsymbol{v}_{RSW} = \frac{\delta \boldsymbol{r}}{\delta t} + \boldsymbol{\omega}_{\mathrm{p}} \times \boldsymbol{r} = \begin{pmatrix} \dot{x} \\ \dot{y} \\ \dot{z} \end{pmatrix} + \begin{pmatrix} 0 \\ 0 \\ n \end{pmatrix} \times \begin{pmatrix} x \\ y \\ z \end{pmatrix} = \begin{pmatrix} \dot{x} - ny \\ \dot{y} + nx \\ \dot{z} \end{pmatrix} \tag{2.74}$$

Finally,

$$\begin{cases} \Delta v_x = -(2\dot{y}_0 + 3nx_0)\sin nt - \dot{x}_0 \cos nt + 3n(\dot{y}_0 + 2nx_0)t + (2\dot{x}_0 - ny_0) \\ \Delta v_y = -\dot{x}_0 \sin nt + (2\dot{y}_0 + 3nx_0)\cos nt - (\dot{y}_0 + 2nx_0) \\ \Delta v_z = -nz_0 \sin nt + \dot{z}_0 \cos nt \end{cases} \tag{2.75}$$

Equation (2.75), together with Eq. (2.67), gives analytical expressions of error changes between orbit prediction values and their truth values, providing that initial position and velocity errors are already known.

If we combine the analytic expression (2.67) for position errors of C-W equation and the analytic expression (2.75) for its velocity errors together, we can write them into a state transition matrix. From Eq. (2.74) we can get

$$\dot{x} = \Delta v_x + ny, \dot{y} = \Delta v_y - nx \tag{2.76}$$

The relation between the state vector of errors $(x, y, z, \dot{x}, \dot{y}, \dot{z})^{\mathrm{T}}$ and the state vector of errors $\left(x, y, z, \Delta v_x, \Delta v_y, \Delta v_z\right)^{\mathrm{T}}$ is

$$\begin{bmatrix} x \\ y \\ z \\ \dot{x} \\ \dot{y} \\ \dot{z} \end{bmatrix} = \begin{bmatrix} 1 & 0 & 0 & 0 & 0 & 0 \\ 0 & 1 & 0 & 0 & 0 & 0 \\ 0 & 0 & 1 & 0 & 0 & 0 \\ 0 & n & 0 & 1 & 0 & 0 \\ -n & 0 & 0 & 0 & 1 & 0 \\ 0 & 0 & 0 & 0 & 0 & 1 \end{bmatrix} \begin{bmatrix} x \\ y \\ z \\ \Delta v_x \\ \Delta v_y \\ \Delta v_z \end{bmatrix} = \boldsymbol{M}_{\mathrm{abs}\to\mathrm{rel}}(n) \begin{bmatrix} x \\ y \\ z \\ \Delta v_x \\ \Delta v_y \\ \Delta v_z \end{bmatrix} \tag{2.77}$$

Thus, the state transition matrix of state vector of error $\boldsymbol{X}(t) = \left(x, y, z, \Delta v_x, \Delta v_y, \Delta v_z\right)^{\mathrm{T}}$ is

$$\boldsymbol{\Phi}(t) = \begin{bmatrix} 2 - \cos nt & \sin nt & 0 & \frac{1}{n}\sin nt & \frac{2}{n}(1 - \cos nt) & 0 \\ 2\sin nt - 3nt & 2\cos nt - 1 & 0 & \frac{2}{n}(\cos nt - 1) & \frac{4}{n}\sin nt - 3t & 0 \\ 0 & 0 & \cos nt & 0 & 0 & \frac{1}{n}\sin nt \\ n(3nt - \sin nt) & n(1 - \cos nt) & 0 & 2 - \cos nt & 3nt - 2\sin nt & 0 \\ n(\cos nt - 1) & -n\sin nt & 0 & -\sin nt & 2\cos nt - 1 & 0 \\ 0 & 0 & -n\sin nt & 0 & 0 & \cos nt \end{bmatrix} \tag{2.78}$$

The expression of state transition matrix $\boldsymbol{\Phi}(t)$ given in reference [38] is inaccurate, for it is a transition matrix from the initial state vector $(x_0, y_0, z_0, \dot{x}_0, \dot{y}_0, \dot{z}_0)^{\mathrm{T}}$ to the terminal state vector $\left(x, y, z, \Delta v_x, \Delta v_y, \Delta v_z\right)^{\mathrm{T}}$. $\boldsymbol{\Phi}(t)$, multiplied by the matrix in Eq. (2.77) to its right, can get the transition matrix from $(x_0, y_0, z_0, \Delta v_{x0}, \Delta v_{y0}, \Delta v_{z0})^{\mathrm{T}}$ to its terminal state $\left(x, y, z, \Delta v_x, \Delta v_y, \Delta v_z\right)^{\mathrm{T}}$.

If we have already known the error vector of initial state $\boldsymbol{X}_0$, the state vector of error at any time t can be solved using the following equation

$$\boldsymbol{X}(t) = \boldsymbol{\Phi}(t)\boldsymbol{X}_0 \tag{2.79}$$

Suppose that $\boldsymbol{P}_0$ is the error covariance matrix in RSW coordinate system at the initial time t0, then the covariance matrix at any time t is

$$\boldsymbol{P}(t) = \boldsymbol{\Phi}(t) \cdot \boldsymbol{P}_0 \cdot \boldsymbol{\Phi}^{\mathrm{T}}(t) \tag{2.80}$$

If initial covariance matrix $\boldsymbol{P}_0$ is diagonal matrix,

$$\boldsymbol{P}_0 = \mathrm{diag}\begin{pmatrix} \sigma_{x0}^2 & \sigma_{y0}^2 & \sigma_{z0}^2 & \sigma_{v_x0}^2 & \sigma_{v_y0}^2 & \sigma_{v_z0}^2 \end{pmatrix} \tag{2.81}$$

Substitute it into Eq. (2.80) and use Eq. (2.78), we can solve the covariance matrix at any time t

$$\boldsymbol{P}(t) = \begin{bmatrix} \boldsymbol{P}_{\mathrm{rr}}(t) & \boldsymbol{P}_{\mathrm{rv}}(t) \\ \boldsymbol{P}_{\mathrm{rv}}^{\mathrm{T}}(t) & \boldsymbol{P}_{\mathrm{vv}}(t) \end{bmatrix} \tag{2.82}$$

where, $\boldsymbol{P}_{rr}(t)$, $\boldsymbol{P}_{rv}(t)$, and $\boldsymbol{P}_{vv}(t)$ stand for position covariance matrix, cross correlation matrix of position and velocity, and velocity covariance matrix, respectively. Refer to Appendix B for their specific expressions. In addition, Ref. [38] points out that the covariance matrix at any time t is a diagonal matrix, so that the conclusion is inaccurate.

The following is the expression of the diagonal element of $\boldsymbol{P}(t)$:

$$\begin{cases} \sigma_x^2(t) = (\cos nt - 2)^2\sigma_{x0}^2 + \sin^2 nt\sigma_{y0}^2 + \dfrac{\sin^2 nt}{n^2}\sigma_{v_x0}^2 + \dfrac{4(1-\cos nt)^2}{n^2}\sigma_{v_y0}^2 \\ \sigma_y^2(t) = (2\sin nt - 3nt)^2\sigma_{x0}^2 + (2\cos nt - 1)^2\sigma_{y0}^2 + \dfrac{4(1-\cos nt)^2}{n^2}\sigma_{v_x0}^2 \\ \qquad + \left(\dfrac{4}{n}\sin nt - 3t\right)^2\sigma_{v_y0}^2 \\ \sigma_z^2(t) = \cos^2 nt\sigma_{z0}^2 + \dfrac{1}{n^2}\sin^2 nt\sigma_{v_z0}^2 \\ \sigma_{v_x}^2(t) = n^2(\sin nt - 3nt)^2\sigma_{x0}^2 + n^2(\cos nt - 1)^2\sigma_{y0}^2 + (2-\cos nt)^2\sigma_{v_x0}^2 \\ \qquad + (3nt - 2\sin nt)^2\sigma_{v_y0}^2 \\ \sigma_{v_y}^2(t) = n^2(1-\cos nt)^2\sigma_{x0}^2 + n^2\sin^2 nt\sigma_{y0}^2 + \sin^2 nt\sigma_{v_x0}^2 \\ \qquad + (2\cos nt - 1)^2\sigma_{v_y0}^2 \\ \sigma_{v_z}^2(t) = n^2\sin^2 nt\sigma_{z0}^2 + \cos^2 nt\sigma_{v_z0}^2 \end{cases} \tag{2.83}$$

Thus, by C-W equations, we can get the analytic propagation function of the initial error covariance matrix. From Eq. (2.83) we can know that, under assumptions of C-W equations, the initial error propagation of nearly circular orbit possesses the following characteristics:

(1) Periodic oscillations exist in errors at all directions (positions and velocities).
(2) Errors along direction W are independent to those in the orbital plane (along direction R and S) so that the errors can be resolved in the orbital plane and along the normal direction, respectively;
(3) Errors along direction W do not have any constant terms, only sine and cosine function terms, which define free oscillations of errors along direction W;
(4) Except for oscillation terms, position errors along direction $S(\sigma_y^2)$, velocity errors along direction $R(\sigma_{v_x}^2)$ and the polynomial term of time t explain that their errors will increase with time and cause error divergence.

(2) Example of verification

We choose four typical objects as calculation examples to verify the orbital initial error propagation analytic formula based on the relative motion theory. See Table 2.3 for type of objects and orbits. See Tables 2.4 and 2.5 for orbital elements of objects as well as position and velocity coordinates in ECI coordinate system (Coordinated Universal Time is 2012-01-01 00:00:00.00 UTC).

Table 2.3 Types of objects and orbits

No.	Type of orbit	Type of object	Object name	Object code
①	Low Earth orbit (LEO)	Earth Resources Satellite	ERS-2	23560
②	Medium Earth orbit (MEO)	GLONASS Satellite	COSMOS 1948	19165
③	Geostationary Earth orbit (GEO)	Galaxy Communication Satellite	Galaxy-11	26038
④	Highly elliptical orbit (HEO)	Molnyia Satellite	Molnyia 3-35	20052

Table 2.4 Orbital elements of objects

No.	a/km	e	i/(°)	Ω /(°)	ω /(°)	M/(°)
①	7151.799943	0.002586	98.618	77.249	76.679	177.919
②	25507.551932	0.000375	64.354	242.658	306.373	53.654
③	42166.577215	0.000036	0.068	109.622	217.823	41.434
④	25663.740026	0.740361	63.463	359.792	270.021	40.168

Table 2.5 Position and velocity coordinates in ECI coordinate system

No.	X/km	Y/km	Z/km	V_x/(km/s)	V_y/(km/s)	V_z/(km/s)
①	−1430.331391	−1627.484800	−6835.083611	1.295564	7.067381	−1.954642
②	−11702.734586	−22658.145307	24.604748	1.521520	−0.783326	3.564419
③	41659.812155	6510.137799	−49.166290	−0.474640	3.037799	−0.000680
④	17110.947418	6872.467973	13886.072215	0.405454	1.938054	3.883779

Suppose that the standard deviation of position errors along each axis directions in *RSW* coordinate system at an initial time is 100 m and the standard deviation of velocity errors is 0.1 m/s, the initial covariance matrix will be

$$\boldsymbol{P}_0 = \mathrm{diag}\left(10^4 \quad 10^4 \quad 10^4 \quad 10^{-2} \quad 10^{-2} \quad 10^{-2}\right) \tag{2.84}$$

In order to verify the correctness of Eq. (2.82), we use the following three methods to analyze the initial error propagation:

(1) The HPOP model in STK software, 21 × 21 order WGS84_EGM96 model of earth gravitation, air drag coefficient 2.2, surface-mass ratio 0.02 m^2/kg, Jacchia-Roberts model of atmospheric density, solar radiation pressure coefficient 1.0. We also choose 21 × 21 order of gravitational field for the covariance calculation in HPOP model. This method only gives position error covariance, hereinafter referred to as HPOP.
(2) The Monte-Carlo method considering only the two-body problem of which the number of sample points is $n_{\text{M-C}} = 10^4$, hereinafter referred to as M-C.
(3) Error propagation analytic formula based on C-W equation, hereinafter referred to as C-W.

The time steps in three methods are all 1 min. It is necessary to illustrate that there are two approaches to generate initial random state with Monte-Carlo method. In the first approach, we generate random sample points at time t_0 which follow the distribution of initial errors then predict these sample points to each time t_i (i = 1, 2, …) using a two-body orbital model. We calculate the covariance of sample prediction values at each time t_i to get information of errors at that time. In the other approach, we regenerate $n_{\text{M-C}}$ initial sample points at time t_0 when we calculate sample prediction values at time t_i. Results of both approaches are basically the same, while the first one gets a smoother standard deviation propagation curve. If we consider from the aspect of analyzing initial error propagation, the first one can explain the changes of initial errors at each time better. Thus we choose the first approach to perform the Monte-Carlo statistical test.

See Figs. 2.11, 2.12 and 2.13 for error standard deviation divergence of three objects (objects ①–③) on nearly circular orbits in *RSW* coordinate system. We can learn that position errors along direction S and velocity errors along direction R on nearly circular orbit have divergences as time passes. Position and velocity errors along other directions have periodic oscillations as time passes without any divergences.

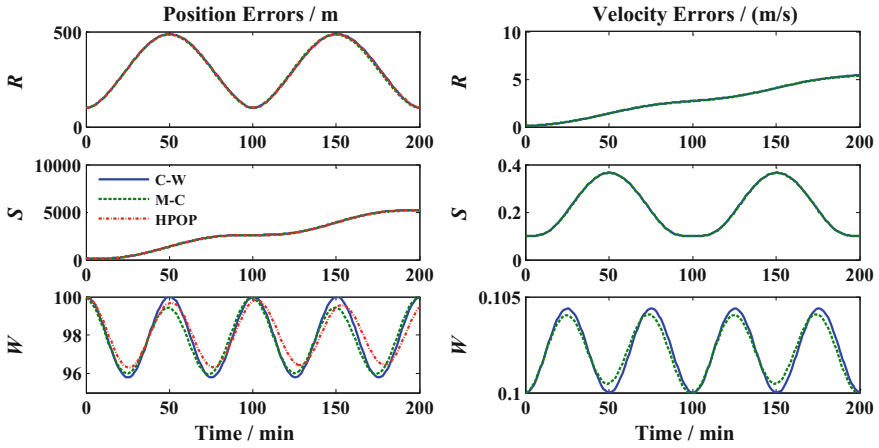

Fig. 2.11 Propagation curve of error standard deviations of object ①

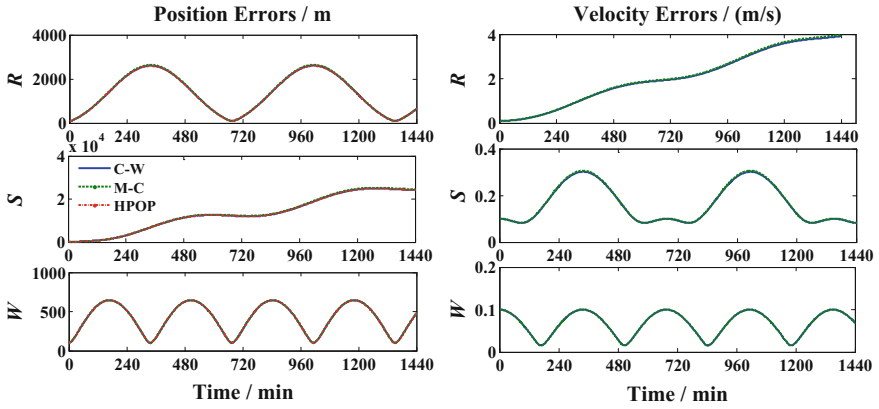

Fig. 2.12 Propagation curve of error standard deviations of object ②

Error standard deviation curves we get from the three methods in Figs. 2.11, 2.12 and 2.13 are very close and hard to distinguish. In order to analyze precisions with C-W method, we list relative error curves with C-W, M-C and HPOP methods in Figs. 2.14 2.15 and 2.16.

We can learn from the derivational process of C-W equation that there are three approximate hypotheses if we describe relative motion of nearly circular orbits with C-W Eq. (2.66). The first one is perturbation force hypothesis, in which the two objects are considered with the same perturbation force and their difference is zero. The second one is linear hypothesis, in which the relative distance of the two objects is considered as a smaller value comparing to their geocentric distance and the equation can be linearized. The third one is the circular orbit hypothesis, in

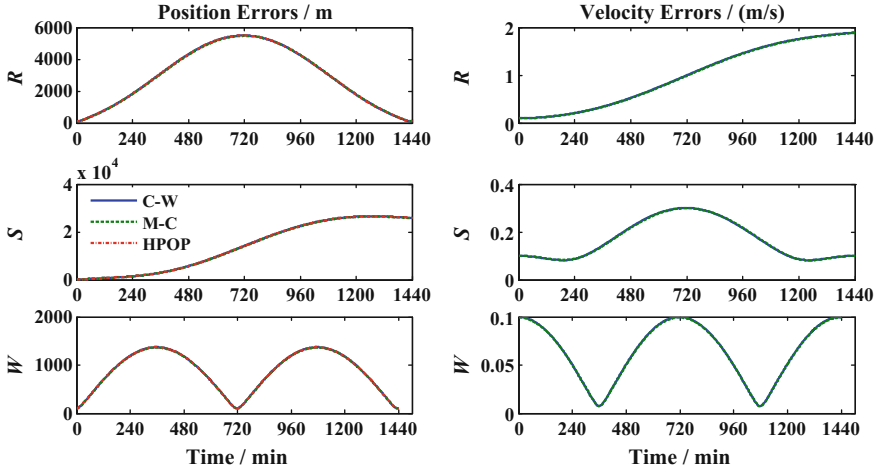

Fig. 2.13 Propagation curve of error standard deviations of object ③

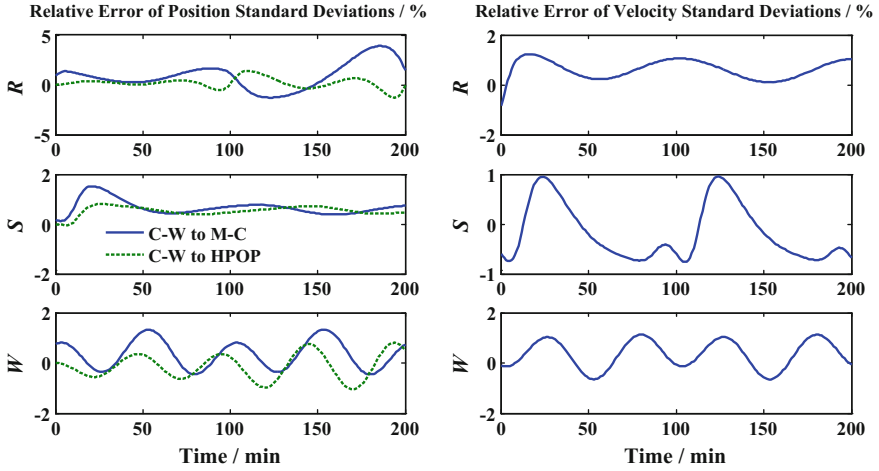

Fig. 2.14 Relative error curve of standard deviations of object ①

which the dominating object orbit is considered as strict circle and the equation can be converted into constant coefficient linear equation.

Likewise, analysis on nearly circular orbital error propagation with C-W equation is also affected by these three hypotheses. In Figs. 2.11, 2.12 and 2.13, deviations among C-W curves and M-C curves reveal deviations caused by linear and circular orbit hypotheses, while deviations among C-W curves and HPOP curves reveal deviations caused by the perturbation force hypothesis. If we analyze the comparison of results in Figs. 2.14, 2.15 and 2.16, we can find that the relative

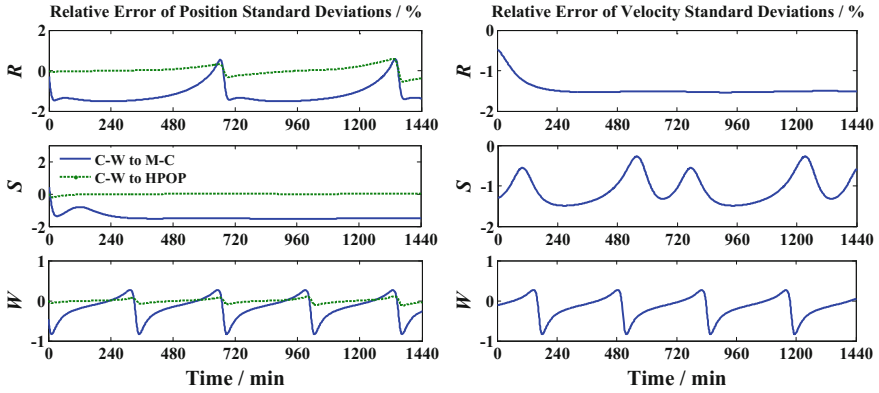

Fig. 2.15 Relative error curve of standard deviations of object ②

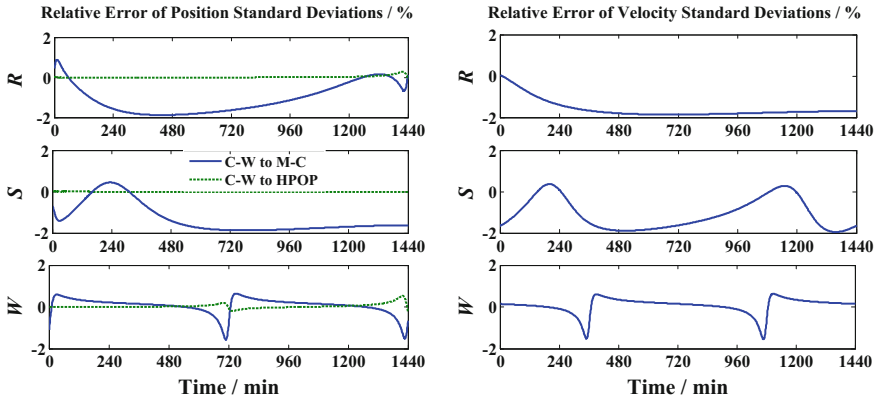

Fig. 2.16 Relative error curve of standard deviations of object ③

errors of results with C-W method are usually no large than 2% comparing with those with M-C and HPOP methods, which indicates that the precision of analyzing initial errors with C-W equation is adequate.

From Fig. 2.11 we can learn that deviation of error standard deviation of object ① along direction *W* is relatively larger, which is due to its relatively smaller amplitude of variation. From Fig. 2.14 we can see that relative errors of object ① along direction *W* are smaller than 2%, no larger than that of other directions.

The relative errors are very small using C-M method and HPOP method in Figs. 2.14, 2.15 and 2.16. We can learn from the derivational process of C-W equation that two-body assumption is not introduced. The assumption is that perturbation forces are the same acting upon the dominating and subordinate objects and that the difference of perturbation forces is zero. When applied to error analysis, it can be seen as that the models of "actual" and prediction orbits are the same and

without any errors. Therefore, on the premise that C-W equation assumption has been met, what orbital model we choose has little to do with the results, which also explains that C-W equation is a good tool for initial error propagation analysis.

3. Error propagation of elliptical orbit based on T-H equation

(1) Error propagation formula

Likewise, the velocity component of prediction errors we get from Eq. (2.72) is relative velocity errors, or it can be seen as time derivative of relative position errors, whereas the projection of absolute velocity errors in the reference orbital coordinate system needs to be concerned. If we take $\boldsymbol{\Phi}(t)$ for the state transition matrix of initial error propagation after its conversion to absolute velocity errors, it can be written as follows according to Eqs. (2.72), (2.74), and (2.76).

$$\begin{aligned}\boldsymbol{\Phi}(t) &= \boldsymbol{M}_{\text{rel}\to\text{abs}}(\omega)\boldsymbol{T}(t)\boldsymbol{M}_{\text{abs}\to\text{rel}}(\omega_0)\\ &= \begin{bmatrix} t_{11}-\omega_0 t_{15} & t_{12}+\omega_0 t_{14} & 0 & t_{14} & t_{15} & 0\\ t_{21}-\omega_0 t_{25} & t_{22}+\omega_0 t_{24} & 0 & t_{24} & t_{25} & 0\\ 0 & 0 & t_{33} & 0 & 0 & t_{36}\\ t_{41}-\omega\ t_{21}-\omega_0(t_{45}-\omega t_{25}) & t_{42}-\omega\ t_{22}+\omega_0(t_{44}-\omega t_{24}) & 0 & t_{44}-\omega\ t_{24} & t_{45}-\omega\ t_{25} & 0\\ t_{51}+\omega\ t_{11}-\omega_0(t_{55}+\omega t_{15}) & t_{52}+\omega\ t_{12}+\omega_0(t_{54}+\omega t_{14}) & 0 & t_{54}+\omega\ t_{14} & t_{55}+\omega\ t_{15} & 0\\ 0 & 0 & t_{63} & 0 & 0 & t_{66}\end{bmatrix}\end{aligned} \tag{2.85}$$

If initial covariance matrix $\boldsymbol{P}_0$ is a diagonal matrix as in Eq. (2.81), we can get covariance matrix $\boldsymbol{P}(t) = \boldsymbol{\Phi}(t)\boldsymbol{P}_0\boldsymbol{\Phi}^{\mathrm{T}}(t)$ at any time t. Refer to Appendix B for the specific expression of covariance matrix $\boldsymbol{P}(t)$. Here we have the expression of its diagonal element.

$$\begin{cases}\sigma_x^2(t) = (t_{11}-\omega_0 t_{15})^2\sigma_{x0}^2 + (t_{12}+\omega_0 t_{14})^2\sigma_{y0}^2 + t_{14}^2\sigma_{v_x0}^2 + t_{15}^2\sigma_{v_y0}^2\\ \sigma_y^2(t) = (t_{21}-\omega_0 t_{25})^2\sigma_{x0}^2 + (t_{22}+\omega_0 t_{24})^2\sigma_{y0}^2 + t_{24}^2\sigma_{v_x0}^2 + t_{25}^2\sigma_{v_y0}^2\\ \sigma_z^2(t) = t_{33}^2\sigma_{z0}^2 + t_{36}^2\sigma_{v_z0}^2\\ \sigma_{v_x}^2(t) = [t_{41}-\omega\ t_{21}-\omega_0(t_{45}-\omega t_{25})]^2\sigma_{x0}^2 + (t_{44}-\omega\ t_{24})^2\sigma_{v_x0}^2\\ \qquad\quad + [t_{42}-\omega\ t_{22}+\omega_0(t_{44}-\omega t_{24})]^2\sigma_{y0}^2 + (t_{45}-\omega\ t_{25})^2\sigma_{v_y0}^2\\ \sigma_{v_y}^2(t) = [t_{51}+\omega\ t_{11}-\omega_0(t_{55}+\omega t_{15})]^2\sigma_{x0}^2 + (t_{54}+\omega\ t_{14})^2\sigma_{v_x0}^2\\ \qquad\quad + [t_{52}+\omega\ t_{12}+\omega_0(t_{54}+\omega t_{14})]^2\sigma_{y0}^2 + (t_{55}+\omega\ t_{15})^2\sigma_{v_y0}^2\\ \sigma_{v_z}^2(t) = t_{63}^2\sigma_{z0}^2 + t_{66}^2\sigma_{v_z0}^2\end{cases} \tag{2.86}$$

In which, t_{ij} is defined by orbital eccentricity e, true anomaly θ, and other elements. Refer to Appendix A for its specific expression. So we can get the explicit propagation functions of initial error covariance by the state transition matrix of elliptical orbits.

If we analyze propagation characteristics of initial errors, we should consider whether there are any divergences with time. Therefore, we divide propagation functions of initial error covariance into long-term items and periodic items for separate observations. The long-term items will cause error divergences whereas the periodic items will only make error oscillations within a certain scope. In order to see clearly the impacts of long-term and short items on initial error propagation, we rewrite coefficients of each item in Eq. (2.86) into the following:

$$t_{ij} = a_{ij}J + \Gamma_{ij}, \quad i,j = 1,2,\cdots,6 \tag{2.87}$$

where $J = k^2(t - t_0)$ is a long-term item changing with time; a_{ij} is the coefficient of the long-term items; Γ_{ij} is the coefficient of the periodic items.

Therefore, we can rewrite the explicit propagation functions of initial error covariance into

$$\begin{cases}
\sigma_x^2(t) = [a_{11}J + \Gamma_{11} - \omega_0(a_{15}J + \Gamma_{15})]^2\sigma_{x0}^2 + [a_{12}J + \Gamma_{12} + \omega_0(a_{14}J + \Gamma_{14})]^2\sigma_{y0}^2 \\
\qquad + (a_{14}J + \Gamma_{14})^2\sigma_{v_x0}^2 + (a_{15}J + \Gamma_{15})^2\sigma_{v_y0}^2 \\
\sigma_y^2(t) = [a_{21}J + \Gamma_{21} - \omega_0(a_{25}J + \Gamma_{25})]^2\sigma_{x0}^2 + [a_{22}J + \Gamma_{22} + \omega_0(a_{24}J + \Gamma_{24})]^2\sigma_{y0}^2 \\
\qquad + (a_{24}J + \Gamma_{24})^2\sigma_{v_x0}^2 + (a_{25}J + \Gamma_{25})^2\sigma_{v_y0}^2 \\
\sigma_z^2(t) = \Gamma_{33}^2\sigma_{z0}^2 + \Gamma_{36}^2\sigma_{v_z0}^2 \\
\sigma_{v_x}^2(t) = [a_{41}J + \Gamma_{41} - \omega(a_{21}J + \Gamma_{21}) - \omega_0(a_{45}J + \Gamma_{45} - \omega(a_{25}J + \Gamma_{25}))]^2\sigma_{x0}^2 \\
\qquad + (a_{44}J + \Gamma_{44} - \omega\ (a_{24}J + \Gamma_{24}))^2\sigma_{v_x0}^2 \\
\qquad + [a_{42}J + \Gamma_{42} - \omega\ (a_{22}J + \Gamma_{22}) + \omega_0(a_{44}J + \Gamma_{44} - \omega(a_{24}J + \Gamma_{24}))]^2\sigma_{y0}^2 \\
\qquad + (a_{45}J + \Gamma_{45} - \omega\ (a_{25}J + \Gamma_{25}))^2\sigma_{v_y0}^2 \\
\sigma_{v_y}^2(t) = [\Gamma_{51} + \omega\ \Gamma_{11} - \omega_0(\Gamma_{55} + \omega\Gamma_{15})]^2\sigma_{x0}^2 + (\Gamma_{54} + \omega\ \Gamma_{14})^2\sigma_{v_x0}^2 \\
\qquad + [\Gamma_{52} + \omega\Gamma_{12} + \omega_0(\Gamma_{54} + \omega\Gamma_{14})]^2\sigma_{y0}^2 + (\Gamma_{55} + \omega\ \Gamma_{15})^2\sigma_{v_y0}^2 \\
\sigma_{v_z}^2(t) = \Gamma_{63}^2\sigma_{z0}^2 + \Gamma_{66}^2\sigma_{v_z0}^2
\end{cases} \tag{2.88}$$

where $a_{5j} + \omega a_{1j} = 0$ ($j = 1, 2, 4, 5$). Taking $j = 1$ for an example, we can prove the following using element values in Appendix A

$$\begin{cases}
\omega = h/r_{\mathrm{T}}^2 = (h/p^2)(1 + e\cos\theta)^2 = k^2(1 + e\cos\theta)^2 = k^2\rho^2 \\
a_{11} = \dfrac{3e\rho_0 s(e^2 + 3\rho_0 - 1)}{\rho(e^2 - 1)} - \dfrac{3e^3 s s_0^2}{\rho\rho_0(e^2 - 1)} \\
a_{51} = \dfrac{3e^3k^2\rho s s_0^2}{\rho_0(e^2 - 1)} - \dfrac{3ek^2\rho\rho_0 s(e^2 + 3\rho_0 - 1)}{e^2 - 1}
\end{cases} \tag{2.89}$$

From Eq. (2.89) we can get

$$a_{51} + \omega a_{11} = 0 \tag{2.90}$$

We can prove other equations in a similar way.

We can get propagation characteristics of elliptical orbit prediction errors using initial error propagation functions in Eq. (2.88):

(1) Position errors along direction R and S in orbits contain long-term item J, which will increase as time passes.
(2) Position errors along direction W in orbits only contain periodic items, which will not have any divergences as time passes.
(3) Velocity errors along direction S and W in orbits will not have any divergences as time passes, whereas velocity errors along direction R will have divergences as time passes because they contain long-term item J.

We can also see from element values of state transition matrix in Annex A that there is eccentricity e in the members of long-term item coefficient a_{1j} (j = 1, 2, 4, 5) of position errors along direction R. Therefore, for circular orbits (e = 0), the long-term item coefficient of position errors along direction R is 0. That is to say, position errors along direction R will not have any divergences with time. In fact, for nearly circular orbits, $e \approx 0$, $\omega \approx n$, Eq. (2.88) can degrade into error propagation function Eq. (2.83) which we get from C-W equation.

(2) Example of verification

We choose typical space objects on highly eccentric orbits (object ④ in Table 2.3) and refer to Tables 2.3, 2.4 and 2.5 for orbital parameters. If we suppose that the standard deviation of position errors along each direction in RSW coordinate system at the initial time is 100 m and the standard deviation of velocity errors is 0.1 m/s, the initial covariance matrix will be consistent with that in Eq. (2.84). We analyze initial error propagation separately using the STK/HPOP model, the Monte-Carlo method which only takes two-body motion into account, and the error propagation analytic formula based on T-H equation, respectively. The time step is 1 min and the number of sample points is nM-C = 104 in the Monte-Carlo method. See Fig. 2.17 for error standard deviation divergence of object ④ in RSW coordination system.

As Object ④ is in an elliptic orbit, it is subject to complicated perturbation factors and with serious error divergences which cause acute changes to its error propagation curve. Position errors along direction R and S and velocity errors along direction R in the orbit continue to increase with time. In the next day, their standard deviations reached at about 30 km, 70 km, and 60 m/s, respectively. Position and velocity errors along other directions caused by initial errors have periodic oscillations as time passes without any divergences.

Error standard deviation curves we get from the three methods in Fig. 2.17 are very close and hard to distinguish. In order to analyze relative errors, we list their curves using T-H, M-C, and HPOP methods in Fig. 2.18.

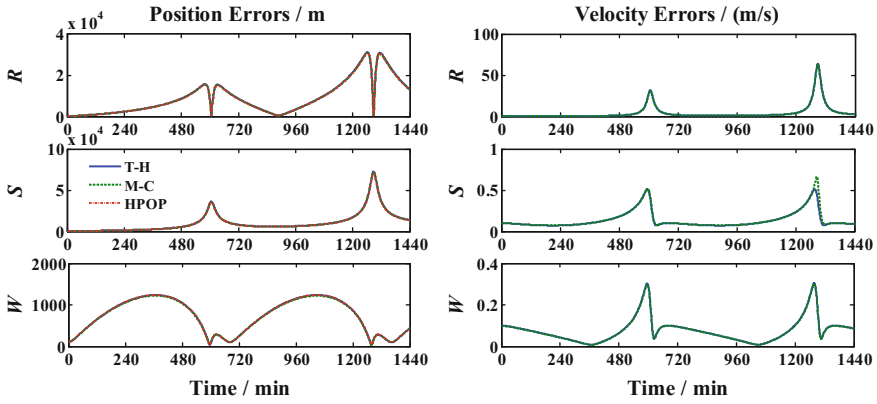

Fig. 2.17 Propagation curve of error standard deviations of object ④ (in RSW coordination system)

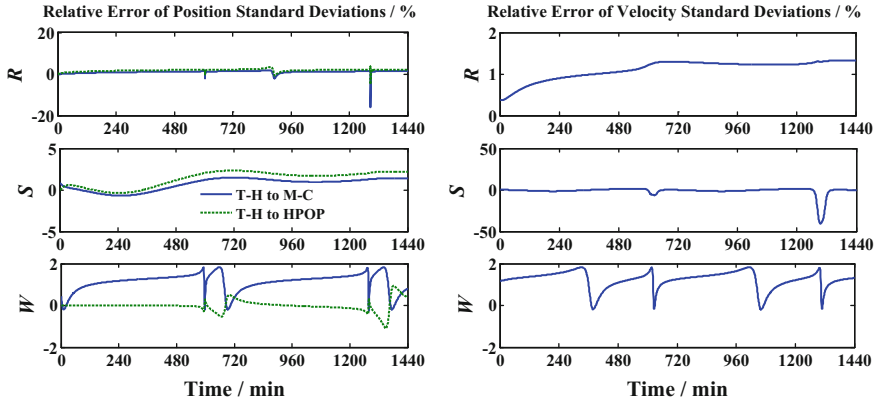

Fig. 2.18 Relative error curve of standard deviations of object ④ (in RSW coordination system)

From Figs. 2.17 and 2.18 we can learn that there is great difference between M-C and T-H curves at around 1290 s for standard deviations of velocity errors along direction *S*. The relative error reaches to 40% when objects are near the perigee. The possible reasons are that the curvature of elliptical orbits is relatively larger near the perigee and that sample points of velocity errors from Monte-Carlo method distribute in arc along orbits as in Fig. 2.19. The error distribution shows non-Gaussian features at that time whereas default errors in calculating error propagation using T-H method accord with Gaussian distribution. If we calculate covariance matrix directly, we may cause larger errors along direction *S* (i.e. the vertical axis in figures).

As in Fig. 2.20, $\boldsymbol{r} = \boldsymbol{r}_s - \boldsymbol{r}_p$ is error vector of the prediction position with respect to the actual position (or the relative position vector from the dominating object to

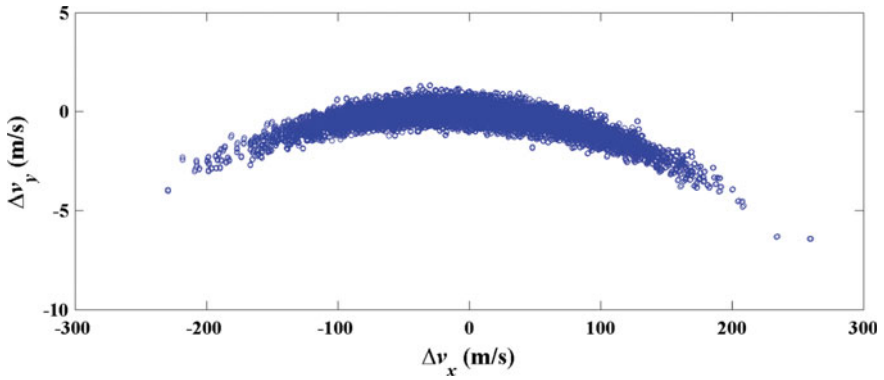

Fig. 2.19 Distribution of velocity errors using Monte-Carlo method at 1290s

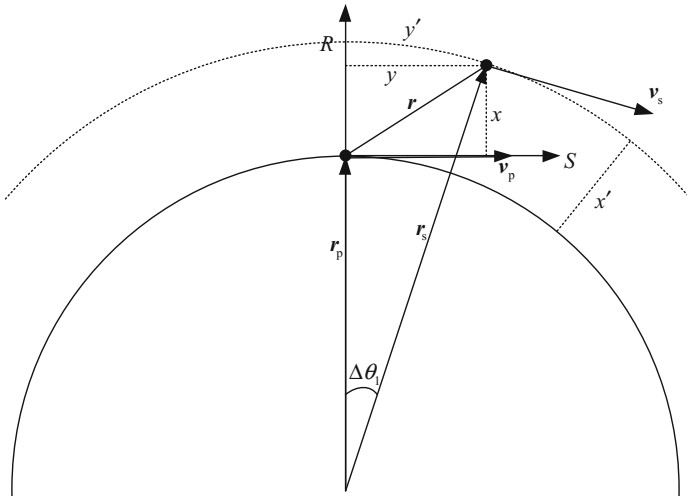

Fig. 2.20 Modifications of error data using orbit curvature

the subordinate object). We can describe error vector $\boldsymbol{r}$ as $\boldsymbol{r} = [x, y, z]^{\mathrm{T}}$ for real positions in *RSW* coordinate system. If we describe errors with the three components $[x, y, z]^{\mathrm{T}}$ in *RSW* coordinate system (a rectangular coordinate system), we can get non-Gaussian distribution errors so that it will be improper to perform error fitting with Gaussian distribution assumption. However, when orbit curvature is not very large, the non-Gaussian features of orbital errors are not obvious. When orbit curvature is comparatively larger (as at the perigee of elliptical orbits), the non-Gaussian features of orbital errors are relatively obvious. We can modify error data using orbit curvature and describe it in a non-rectangular coordinate system.

As in Fig. 2.20, we define a polar coordinate system. The geocenter is taken as its origin and actual position $\boldsymbol{r}_{\mathrm{p}}$ as its initial position. We can use an angle $\Delta\theta_1$ and a

distance $x' = r_s - r_p$ to present the two-dimensional error vector $\boldsymbol{r}$ in the orbital plane, in which $\Delta\theta_1$ stands for a tiny angle between actual and prediction positions of the object. Modified results of error data are $\boldsymbol{r} = [x', y', z']^T$, where x' is the radial distance of prediction position away from its original orbit; y' is front or back deviations of prediction position in orbits; z' is the normal distance of prediction position away from its orbit plane. They can be respectively presented as follows

$$x' = r_s - r_p, \quad y' = r_p \Delta\theta_1, \quad z' = z \tag{2.91}$$

When orbit curvature is comparatively smaller, we can consider $x' = x$ and $y' = y$; when orbit curvature is comparatively larger, differences between x' and x, y' and y become non-negligible. Similarly, differences between velocity errors Δv_y and $\Delta v_y'$ along direction S are also large. Due to the comparatively larger magnitude of position errors (tens of kilometers), it is not obvious in previous simulation results; the comparatively smaller magnitude of velocity errors (tenths of a meter per second), slight changes will cause comparatively larger relative errors. That explains why relative velocity errors are comparatively larger along direction S in Fig. 2.18.

We can modify results from Monte-Carlo method by the following formula:

$$\begin{cases} \Delta\theta_1 = \arctan\left[y/\left(x + r_p\right)\right] \\ x' = \sqrt{y^2 + \left(x + r_p\right)^2} - r_p \\ y' = r_p \Delta\theta_1 \end{cases}, \quad \begin{cases} \Delta\theta_2 = \arctan\left[\Delta v_x/\left(\Delta v_y + v_p\right)\right] \\ \Delta v_x' = v_p \Delta\theta_2 \\ \Delta v_y' = \sqrt{\Delta v_x^2 + \left(\Delta v_y + v_p\right)^2} - v_p \end{cases} \tag{2.92}$$

where $\Delta v_x'$ and $\Delta v_y'$ are velocity errors after modifications; $\Delta\theta_2$ is an angle between the prediction and real velocities.

Figures 2.21 and 2.22 are result curves of standard deviations after we modified error data using orbit curvature. Relative error of standard deviations of velocity

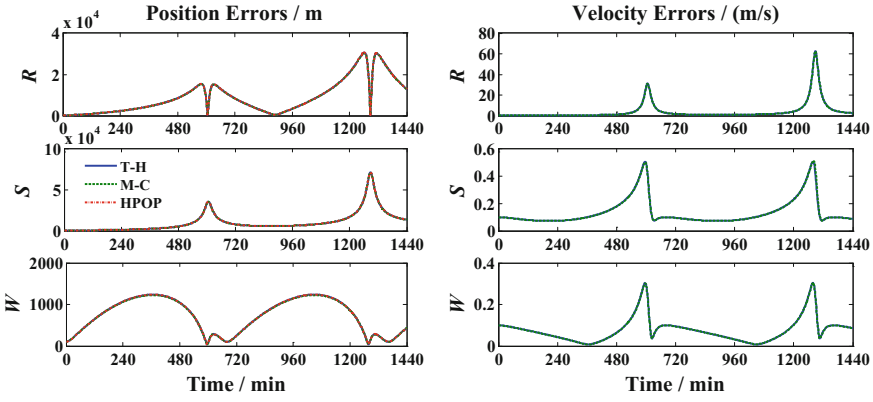

Fig. 2.21 Propagation curve of error standard deviations of object ④ (in RSW coordination system with curvature modifications)

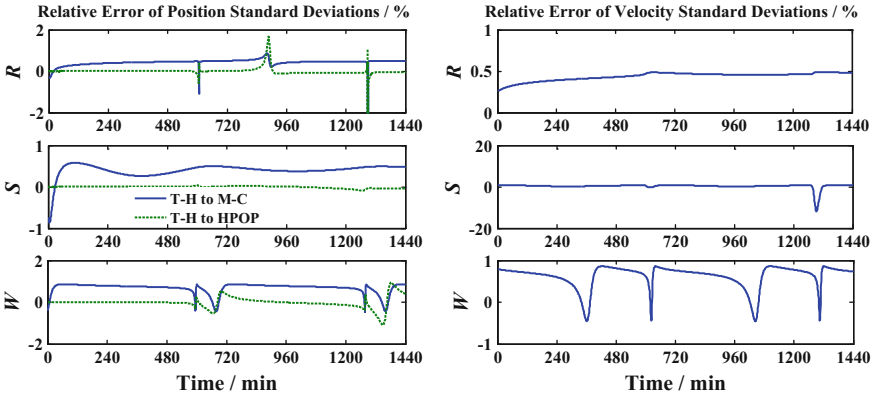

Fig. 2.22 Relative error curve of standard deviations of object ④ (in RSW coordination system with curvature modifications)

errors along direction *S* reduces to 12%. Velocity error magnitude along direction *S* is comparatively smaller, so the absolute error corresponding to the relative error of 12% is very small. The two close curves of standard deviations of velocity errors along direction *S* in Fig. 2.21 also explain that.

We can learn from the derivational process of T-H equation that there are two approximate hypotheses if we describe relative motion. The first one is perturbation force hypothesis, in which the two objects are considered with the same perturbation force and their difference is zero. The second one is linear hypothesis, in which the relative distance of the two objects is considered as a smaller value comparing to their geocentric distances and the equation can be linearized. In the same way, analysis on orbit prediction error propagation with T-H equation is also affected by these two approximate hypotheses. In Figs. 2.27 and 2.21, deviations between T-H and M-C curves reveal deviations caused by linear hypothesis, while deviations between T-H and HPOP curves reveal deviations caused by perturbation force hypothesis. From Fig. 2.22 we can learn that except for the aforementioned particular points, the relative errors between results using T-H method and those of M-C and HPOP methods are usually no more than 2%, which indicates that the precision of analyzing initial errors with T-H equation is adequate.

Due to the relatively large orbital eccentricity and large flight angle of object ④, both *RSW* and *NTW* coordinate systems reflect a relatively obvious difference. The propagation and relative error curves of error standard deviations of *NTW* coordinate system are shown in Figs. 2.23 and 2.24.

From Fig. 2.23 we can learn that error propagation characteristics are different in *NTW* and *RSW* coordinate systems. In *NTW* coordinate system, position errors along direction *T* and velocity errors along direction *N* have divergence as time passes, while position errors along direction *N* have periodic oscillations and velocity errors along direction *T* have divergence as time passes. In addition, the position error curve along direction *R* in Fig. 2.17 has sudden changes near the

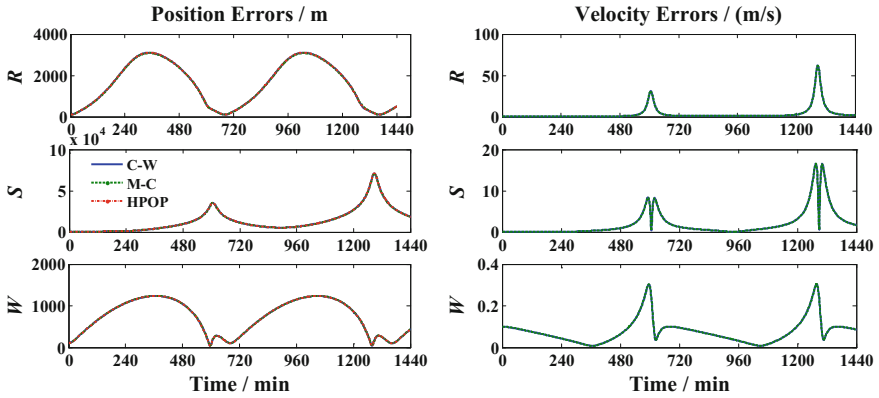

Fig. 2.23 Propagation curve of error standard deviations of object ④ (in NTW coordination system)

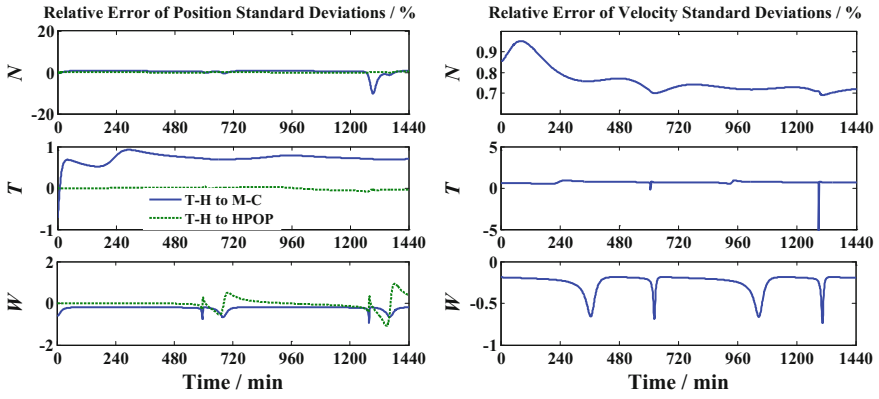

Fig. 2.24 Propagation curve of error standard deviations of object ④ (in NTW coordination system)

perigee and gradually larger amplitude; the position error curve along direction *N* in Fig. 2.23 is relatively smooth and doesn't increase over time, while velocity errors along direction *T* have sudden changes near the perigee. We pay more attention to velocity error propagation in practical applications. Therefore, for highly eccentric orbit, we prefer describing errors using *NTW* coordination system rather than *RSW* coordination system.

We can make qualitative explanations in Fig. 2.25 for the two characteristics of elliptical orbit errors in *RSW* coordinate system along direction *R* (gradually larger amplitude and sudden changes near the perigee). According to theories and practices of orbital dynamics and error propagation [39–41], the long axis of the error ellipsoid is basically identical with the velocity direction, and three principal axis directions are consistent with the three coordinate axis directions in *NTW* coordinate

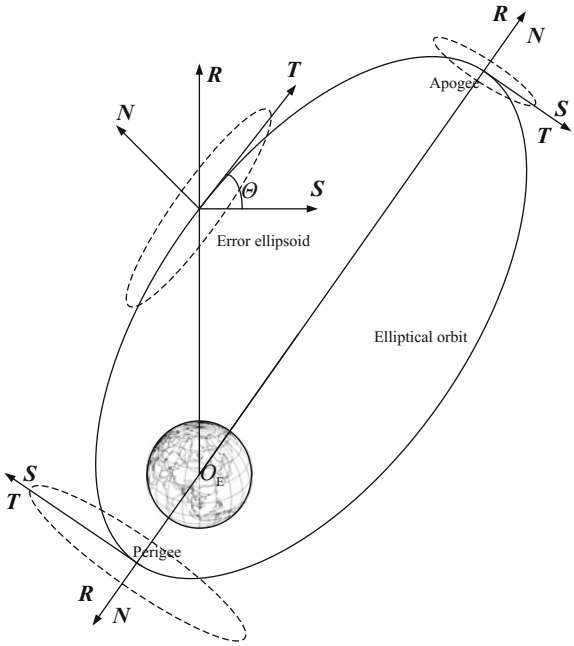

Fig. 2.25 Error ellipsoid of elliptical orbit

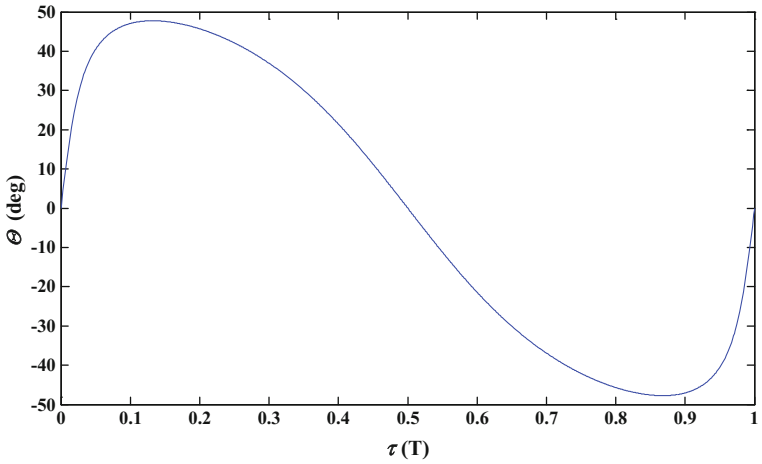

Fig. 2.26 The changing curve of velocity angle Θ of object ④ with its passing the Perigee time τ

system as in Fig. 2.26. The angle between Axis *S* in *RSW* coordinate system and Axis *T* in *NTW* coordinate system is the flight-path angle Θ, which is never zero in orbits except for the perigee and apogee. Therefore, the long axis of error ellipsoid

always has projection on Axis *R* except for the perigee and apogee. As the long axis getting longer over time, the projection enlarges in periodic oscillations, which explains the tendency of long-term position error divergences along direction *R*.

Figure 2.26 is a changing curve of the flight-path angle of object ④ with its passing the perigee time τ, taking the orbital period as the unit of abscissa. From Fig. 2.26 we can notice that the flight-path angle near the perigee changes from a maximum negative value to zero, then to a maximum positive value. The flight-path angle decreases rapidly to zero near the perigee and the projection of the long axis of error ellipsoid along direction *R* also decreases rapidly, which explain why there are sudden changes to the errors near the perigee.

2.4.2 *Correlation Characterization Based on Geometrical Model*

The propagation characteristics of initial error of circular and eccentric orbit are analyzed based on C-W equations and T-H equations respectively in Sect. 2.4.1, which belong to the algebraic model. The negative correlation characteristics of position and velocity error in the case of near-circular orbit are studied based on the geometrical model of relative motion in this section. The application of negative correlation characteristics in the determination of initial error covariance is discussed. The correlation characteristics are validated by historical orbital data.

Orbit prediction error analysis on TLE orbit in Refs. [38, 42] points out that the curve shapes of position errors along S direction and velocity errors along R direction, position errors along R direction and velocity errors along S direction on circular orbit are roughly the same. They are merely inversed around the horizontal axis, which makes them similar. References [38, 42] analyzed this correlation characterization and put forward an assumption that orbit prediction errors are mainly caused by the advancing and falling behind of prediction position on actual orbits, which can explain the generation of long-term error divergences. This assumption only considers the advancing and falling behind of prediction position on actual orbits and does not take the differences between prediction and actual orbits into account. Therefore, it can explain the long-term error divergence characterization, negative correlation characterization of position errors along S direction and velocity errors along R direction, but fails to explain the relation between position errors along R direction and velocity errors along S direction. In this section, we analyze error correlation characterization using geometrical models for relative motion on basis of the references.

Liu has analyzed the correlation characterization of satellite orbital errors [43], derived the relations between satellite position, velocity errors and orbital element errors in RTN frame, provided the quantitative relations between position and

velocity errors in RTN frame on nearly circular orbits and also analyzed the correlation of orbital element errors restrained by position errors in RTN frame.

1. **Geometrical Models for Relative Motion**

Taking orbital elements of the primary and secondary objects as parameters, the relative dynamics equation is built according to space geometry relation to describe relative motion of space objects, which is called geometrical models for relative motion. Since the geometrical method describes relative motion based on orbital elements, we can apply orbital perturbation theory for the study of the influence of perturbation on relative motion. In the geometrical method, we build relative motion models on primary object orbital coordinate system as well. Schaub [44, 45] came up with a method in which geometrical relationship of relative motion is shown by orbital element differences. We make the relative state vector between two objects in the primary RSW coordinate system as

$$\boldsymbol{X} = (x, y, z, \dot{x}, \dot{y}, \dot{z})^{\mathrm{T}} \tag{2.93}$$

The orbital element vector of the primary object and the orbital elements difference vector of the secondary to the primary object are

$$\boldsymbol{e} = (a, e, i, \Omega, \omega, M)^{\mathrm{T}}, \delta\boldsymbol{e} = (\delta a, \quad \delta e, \delta i, \delta\boldsymbol{\Omega}, \delta\omega, \delta M)^{\mathrm{T}} \tag{2.94}$$

Then the relative position and velocity coordinates in terms of the orbital elements differences can be written as

$$\begin{cases} x = \frac{r}{a}\delta a - a\cos f\delta e + \frac{ae\sin f}{\sqrt{1-e^2}}\delta M \\ y = \frac{2+e\cos f}{1+e\cos f}a\sin f\,\delta e + r(\delta\omega + \cos i\,\delta\Omega) + \frac{a^2}{r}\sqrt{1-e^2}\delta M \\ z = r\sin u\delta i - r\cos u\sin i\delta\boldsymbol{\Omega} \\ \dot{x} = -\frac{ne\sin f}{2\sqrt{1-e^2}}\delta a + \frac{a^3}{r^2}\sqrt{1-e^2}n\sin f\delta e + \frac{a^3}{r^2}ne\cos f\,\delta M \\ \dot{y} = -\frac{3a}{2r}n\sqrt{1-e^2}\delta a + \frac{e+2\cos f+e(2+e\cos f)\cos^2 f}{(1-e^2)^{3/2}}an\,\delta e \\ \quad + \frac{ane\sin f}{\sqrt{1-e^2}}(\delta\omega + \cos i\,\delta\boldsymbol{\Omega}) - \frac{a^3}{r^2}ne\sin f\,\delta M \\ \dot{z} = \frac{an}{\sqrt{1-e^2}}(\cos u + e\cos\omega)\delta i + \frac{an\sin i}{\sqrt{1-e^2}}(\sin u + e\sin\omega)\delta\Omega \end{cases} \tag{2.95}$$

where

$$r = \frac{a(1-e^2)}{1+e\cos f}, n = \sqrt{\frac{\mu}{a^3}} \tag{2.96}$$

Equation (2.95) depicts the relative position and velocity in RSW coordinate system using the Keplerian orbital element differences, in which $(\dot{x}, \dot{y}, \dot{z})^{\mathrm{T}}$ is the relative velocity error or the temporal derivative of the relative position error. The projection of absolute velocity error into the orbital coordinate system is what more

concerned in error analysis. From the relation of absolute and relative velocities we can get

$$\Delta v_x = \dot{x} - y\dot{f}, \Delta v_y = \dot{y} + x\dot{f}, \dot{f} = \frac{h}{r^2} = \frac{a^2}{r^2} n\sqrt{1-e^2} \tag{2.97}$$

Therefore

$$\begin{cases} v_x = -\frac{ne\sin f}{2\sqrt{1-e^2}}\delta a - \frac{a^2 n \sin f}{r\sqrt{1-e^2}}\delta e - \frac{a^2 n\sqrt{1-e^2}}{r}(\delta\omega + \cos i\delta\Omega) - \frac{a^3 n}{r^2}\delta M \\ v_y = -\frac{an\sqrt{1-e^2}}{2r}\delta a + \frac{e+\cos f + 2e(2+e\cos f)\cos^2 f}{(1-e^2)^{3/2}} an\delta e \\ \quad + \frac{ane\sin f}{\sqrt{1-e^2}}(\delta\omega + \cos i\delta\Omega) \\ v_z = \frac{an}{\sqrt{1-e^2}}(\cos u + e\cos\omega)\delta i + \frac{an\sin i}{\sqrt{1-e^2}}(\sin u + e\sin\omega)\delta\Omega \end{cases} \tag{2.98}$$

For the near-circular orbit $(e \approx 0, r \approx a)$, if eliminating terms containing eccentricity e in Eqs. (2.95) and (2.98), we can get

$$\begin{cases} x \approx \delta a - a\cos f\delta e \\ y \approx 2a\sin f\delta e + a(\delta\omega + \cos i\delta\Omega + \delta M) \\ z \approx a(\sin u\delta i - \cos u\sin i\delta\Omega) = a\sqrt{\delta i^2 + \sin^2 i\delta\Omega^2}\sin(u - \phi_z) \\ v_x \approx -an\sin f\delta e - an(\delta\omega + \cos i\delta\boldsymbol{\Omega} + \delta M) \\ v_y \approx -\frac{n}{2}\delta a + an\cos f\delta e \\ v_z \approx an(\cos u\delta i + \sin u\sin i\delta\Omega) = an\sqrt{\delta i^2 + \sin^2 i\delta\Omega^2}\sin(u + \phi_{vz}) \end{cases} \tag{2.99}$$

where the phase angles of position and velocity errors along W direction are

$$\phi_z = \arctan\frac{\sin i\delta\Omega}{\delta i}, \quad \phi_{vz} = \arctan\frac{\delta i}{\sin i\delta\Omega} \tag{2.100}$$

Generally, orbital element errors δe, δi, $\delta\Omega$ and $\delta\omega$ are all small values. They don't change over time (two-body) or change over time slowly (perturbation). The error of semi-major axis δa is largely affected by atmospheric drag which makes its changes faster than other orbital elements aforementioned. If we suppose that the semi-major axis error δa has linear variations over time, we can write it as follows

$$\delta a = \delta a_0 + \delta\dot{a}\cdot\tau, \quad \tau = t - t_0 \tag{2.101}$$

Mean anomaly error δM changes fast over time and have the following relation with initial semi-major axis error δa_0 and semi-major axis rate $\delta\dot{a}$:

$$\delta M = \delta M_0 - \frac{3n}{2\alpha}\left(\delta a_0\tau + \frac{\delta\dot{a}}{2}\tau^2\right) \tag{2.102}$$

Substitute Eqs. (2.101) and (2.102) into the terms in the orbital plane of Eq. (2.99), we can get

$$\begin{cases} x \approx \delta\dot{a}\tau - a\cos f\,\delta e + \delta a_0 \\ y \approx \left(-\frac{3}{4}n\delta\dot{a}\tau^2 - \frac{3}{2}n\delta a_0\tau\right) + 2a\sin f\,\delta e + a(\delta\omega + \cos i\,\delta\Omega + \delta M_0) \\ v_x \approx \left(\frac{3}{4}n^2\,\delta\dot{a}\tau^2 + \frac{3}{2}n^2\delta a_0\tau\right) - an\sin f\,\delta e - an(\delta\omega + \cos i\,\delta\Omega + \delta M_0) \\ v_y \approx -\frac{n}{2}\delta\dot{a}\tau + an\cos f\,\delta e - \frac{n}{2}\delta a_0 \end{cases} \tag{2.103}$$

Equation (2.103) reveals that there are linear term τ and quadratic term τ^2 of time in position errors along S direction and velocity errors along R direction, which will have fast divergences as time passes. In position errors along R direction and velocity errors S along direction, there are only linear term τ, initial semi-major axis error δa_0 and eccentricity error δe. Because semi-major axis change rate $\delta\dot{a}$ has a small magnitude, the linear term of time which takes it as parameter has smaller changes over time and not obvious long-term divergences. The position errors and velocity errors along W direction are defined by direction errors of the orbital plane (the inclination error δi and the right ascension of ascending node error $\delta\Omega$), and oscillates with the orbital period. The periodicity of position and velocity errors on the orbital plane (along R and S direction) is caused by eccentricity error δe and its period is also orbital period.

2. Correlation of Position and Velocity Errors

(1) Relations of position and velocity errors along R and S direction

Equation (2.103) indicates that the expression of position error y along S direction and velocity error v_x along R direction is composed by three parts for near-circular orbits:

(1) secular term (up to second order) caused by initial semi-major axis error δa_0 and its change rate $\delta\dot{a}$;
(2) periodic term caused by eccentricity error δe;
(3) constant term caused by argument of perigee error $\delta\omega$, right ascension of the ascending node error $\delta\Omega$ and initial mean anomaly error δM_0.

Position error y along S direction and velocity error v_x along R direction have the following approximate relation:

$$\frac{v_x}{y} \approx -n = -\frac{2\pi}{T} \tag{2.104}$$

Equation (2.103) indicates that the expression of position error x along R direction and velocity error v_y along S direction is also composed by three parts for near-circular orbits:

(1) one-order secular term caused by semi-major axis change rate $\delta\dot{a}$;
(2) periodic term caused by eccentricity error δe;
(3) constant term caused by initial semi-major axis error δa_0.

Position error x along R direction and velocity error v_y along S direction have the following approximate relation:

$$\frac{v_y}{x} \approx -n = -\frac{2\pi}{T} \tag{2.105}$$

Equations (2.104) and (2.105) represent the approximate relations of position and velocity errors along R and S direction for near-circular orbit. For near-circular orbit, quantitative relation is obvious between position and velocity errors along R and S direction:

(1) For magnitude, the R and S components of velocity errors are $n = 2\pi/T$ times than the S and R components of position errors. For LEO, its period $T \approx 100$min, n is about 1/1000; for MEO, its period $T \approx 12$ h, n is approximately 1/7000; for GEO, its period $T \approx 24$ h, n is approximately 1/14,000.
(2) For sign, the sign of the R and S components of velocity errors are opposite to the S and R components of position errors, which explain that the curve shapes of position errors along S direction and velocity errors along R direction on circular orbit are approximately the same. They are merely inversed around the horizontal axis, which makes them similar.

(2) Relations of position and velocity errors along W direction

Position and velocity errors along W direction have periodic oscillations, and their oscillation functions are

$$z \approx a\sqrt{\delta i^2 + \sin^2 i\,\delta\Omega^2}\sin\left(u - \phi_z\right), v_z \approx an\sqrt{\delta i^2 + \sin^2 i\,\delta\Omega^2}\sin\left(u + \phi_{vz}\right) \tag{2.106}$$

Equation (2.100) infers that phase angles of position and velocity errors meet:

$$\phi_z + \phi_{vz} = \frac{\pi}{2} \tag{2.107}$$

Therefore, the v_z expression in Eq. (2.106) can be written as

$$v_z \approx na\sqrt{\delta i^2 + \sin^2 i\delta\Omega^2}\sin\left(u + \frac{\pi}{2} - \phi_z\right) \tag{2.108}$$

The relation of position error z and velocity error v_z along W direction is

$$v_z(u) = nz\left(u + \frac{\pi}{2}\right) = \frac{2\pi}{T} z\left(u + \frac{\pi}{2}\right) \tag{2.109}$$

where $v_z(\cdot)$ and $z(\cdot)$ denote that position and velocity errors are functions of the argument of latitude u. Equation (2.109) represents the approximate relation of position and velocity errors along W direction on near-circular orbit. For amplitude, velocity errors are $n = 2\pi/T$ times than position error. For phase, velocity errors are $\pi/2$ ahead of position errors.

3. **Negative Correlation Characteristic of Error Covariance Matrix**

From the last section we can know that position errors along S direction and velocity errors along R direction are in approximate quantitative relation as in Eq. (2.104), and position errors along R direction and velocity errors along S direction are also in approximate quantitative relation as in Eq. (2.105). This characteristic is actually the negative correlation of position and velocity errors, which reflects in error covariance matrix, i.e. the negative correlation characteristic of covariance matrix. We can use a correlation coefficient to express this inverse relationship and approximate characterization. The definition of correlation coefficient ρ is [46]

$$\rho(X, Y) = \frac{\mathrm{cov}(X, Y)}{\sqrt{\sigma^2(X)\sigma^2(Y)}} \tag{2.110}$$

where $\mathrm{cov}(\cdot, \cdot)$ and $\sigma^2(\cdot)$ are covariance and variance respectively, correlation coefficient is dimensionless.

The absolute value of correlation coefficient ρ is not larger than 1, i.e. $|\rho| \leq 1$. $|\rho|$ getting larger indicates that X and Y have closer connections for linear relation; especially when $|\rho| = 1$, X and Y are in linear relation with probability 1. When $\rho > 0$, X and Y have same tendencies; when $\rho < 0$, X and Y have opposite tendencies. When ρ is near 1, positive linear relation is between two random variables; when ρ is near -1, negative linear relation is between two random variables (negative correlation); when ρ is near 0, no linear relations are between two random variables.

The expression of orbital error covariance matrix $\boldsymbol{P}(t)$ using C-W equations is got in Sect. 2.4.1. The correlation coefficients could be gotten through the following equation:

$$\rho_{x,v_y} = \frac{\mathrm{cov}(x, v_y)}{\sigma(x)\sigma(v_y)} = \frac{P_{1,5}}{\sqrt{P_{1,1}P_{5,5}}}, \quad \rho_{y,v_x} = \frac{\mathrm{cov}(y, v_x)}{\sigma(y)\sigma(v_x)} = \frac{P_{2,4}}{\sqrt{P_{2,2}P_{4,4}}} \tag{2.111}$$

The initial covariance matrix is then propagated, the correlation coefficients are obtained by Eq. (2.111). Figures 2.27, 2.28 and 2.29 illustrate the curves of two correlation coefficients ρ_{x,v_y} and ρ_{y,v_x} of three objects over time. Note that these two correlation coefficients in initial covariance matrix are both zero.

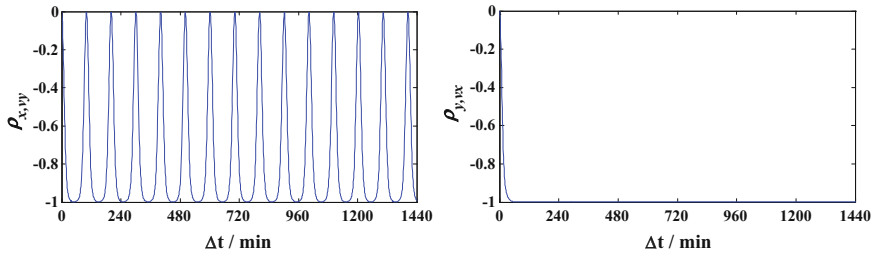

Fig. 2.27 Correlation coefficients of LEO object based on C-W equations

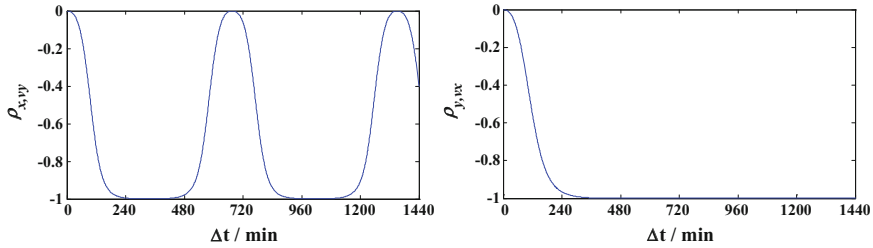

Fig. 2.28 Correlation coefficients of MEO object based on C-W equations

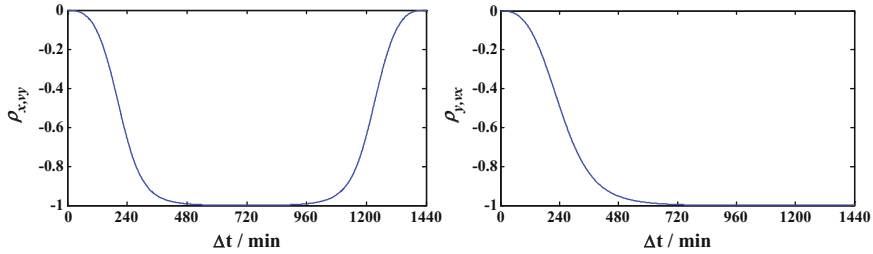

Fig. 2.29 Correlation coefficients of GEO object based on C-W equations

Figures 2.27, 2.28 and 2.29 show that the correlation coefficient ρ_{y,v_x} between position error along S direction and velocity error along R direction changes from 0 to −1 very quickly after the beginning of the prediction (within half an orbital period), which indicates that there is strong negative correlation between position error along S direction and velocity error along R direction. The correlation coefficient ρ_{x,v_y} of position error along S direction and velocity error along R direction is permanently not larger than zero and has oscillations from 0 to −1, with the orbital period. There is also strong negative correlation between position error along R direction and velocity error along S direction.

Table 2.6 Epoch and initial orbital elements

Epoch (UTCG)	a/km	e	i/(°)	Ω /(°)	ω/(°)	M/(°)
2012-07-01 00:00:00.00	7068.920954	0.002805	98.141	256.737	96.061	180.974

Table 2.7 Initial position and velocity covariance matrix

		x	y	z	v_x	v_y	v_z
$\rho = 0$	x	25					
	y		100				
	z			25			
	v_x				4×10^{-4}		
	v_y					1×10^{-4}	
	v_z						1×10^{-4}
$\rho = -0.9$	x	25				−0.045	
	y		100		−0.18		
	z			25			
	v_x		−0.18		4×10^{-4}		
	v_y	−0.045				1×10^{-4}	
	v_z						1×10^{-4}
$\rho = 0.9$	x	25				0.045	
	y		100		0.18		
	z			25			
	v_x		0.18		4×10^{-4}		
	v_y	0.045				1×10^{-4}	
	v_z						1×10^{-4}

4. Application of Correlation Characteristic in Error Propagation

One of the applications of the negative correlation characteristic of orbital error is the determination of initial error covariance matrix. A LEO object is taken as an example to explain. Table 2.6 shows the epoch and initial orbital elements.

Three conditions are considered when determine the initial covariance matrix: (1) the position and velocity errors are non-correlated; (2) the position and velocity errors are in negative correlation, the correlation coefficients $\rho_{x,v_y} = \rho_{y,v_x} = -0.9$; (3) the position and velocity errors are in positive correlation, the correlation coefficients $\rho_{x,v_y} = \rho_{y,v_x} = 0.9$. Table 2.7 shows the initial position and velocity covariance matrix under these three conditions.

We use high precision orbit propagation (HPOP) models to perform orbit propagation and covariance propagation. Under the three initial covariance conditions, we use the STK/HPOP covariance propagation module to perform initial error covariance matrix prediction and get changing curves of error standard deviations of one-day and ten-day predictions in RSW coordination system as in

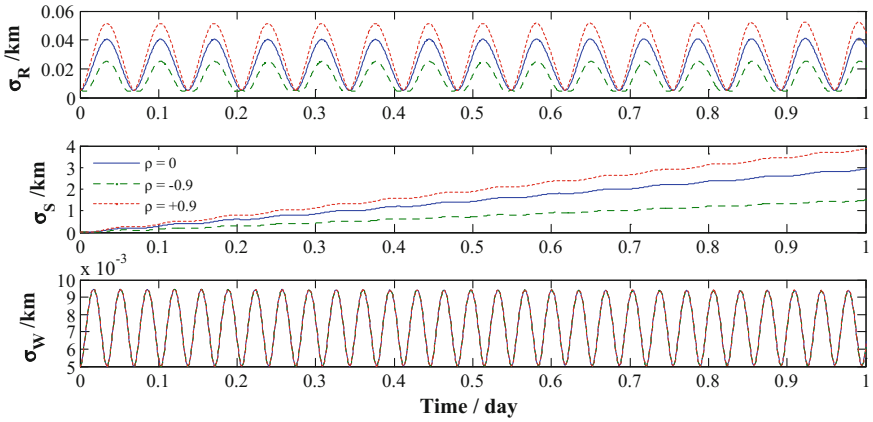

Fig. 2.30 Propagation of initial covariance (1 day)

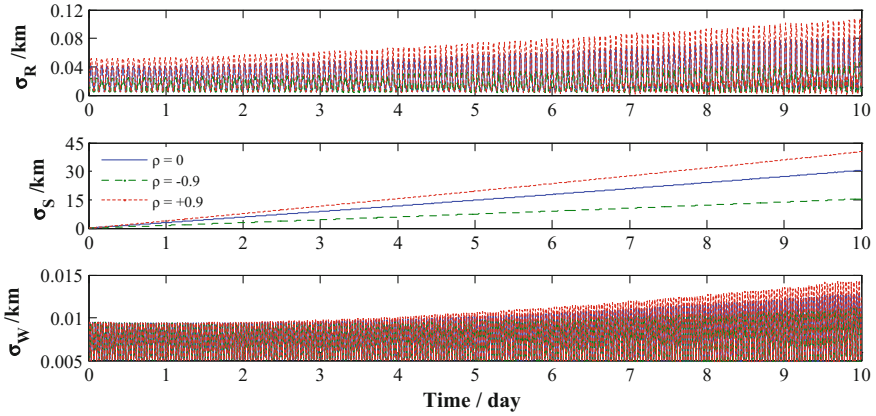

Fig. 2.31 Propagation of initial covariance (10 day)

Figs. 2.30 and 2.31. These figures indicate that the consideration of negative correlation characteristic of position and velocity errors when determining initial covariance can obviously reduce the divergence of initial error.

The negative correlation characteristic of position and velocity errors is derived under the assumption that the orbit is near-circular and the orbital element error are small values. If the errors of near-circular orbit do not meet negative correlation characteristics, the orbital element error is not a small value and orbit prediction errors must have serious divergence. Due to the internal relations among position and velocity errors at all directions, we must consider the relations when defining initial covariance matrix to make sure that the parameters are self-consistent and reasonable.

References

1. Liu L (2000) Orbit theory of spacecraft. National Defense Industry Press, Beijing
2. Vallado DA (2004) Fundamentals of astrodynamics and applications, 2nd edn. Microcosm Press, El Segundo
3. CCSDS Secretariat. Draft recommendation for space data system standards: Conjunction Data Message. Draft recommended standard CCSDS 508.0-R-1, 2012
4. Li JS (2003) Orbit determination of spacecrafts. National Defense Industry Press, Beijing
5. Gelb A, Warren RS (1972) Direct statistical analysis of nonlinear system—CADET. In: AIAA guidance and control conference, pp 72–875
6. Taylor JH, Price CF (1974) Direct statistical analysis of missile guidance systems via CADET. Analytic Sciences Corporation, Massachusetts
7. Taylor JH (1975) Handbook for the direct statistical analysis of missile guidance system via CADET. Analytic Sciences Corporation, Massachusetts
8. Gelb A, Kasper J, Price C et al (1974) Applied optimal estimation. MIT Press, Cambridge, MA
9. Liang LB, Luo YZ, Zhang J et al (2010) Rendezvous—phasing errors propagation using quasi—linearization method. In: AIAA2010-7594. AIAA guidance, navigation, and control conference, Toronto, Ontario
10. Liang LB, Luo YZ, Xing JJ et al (2010) Precision analysis of nonlinear rendezvous by covariance analysis description equation technique. Syst Eng Electron 32(9):1977–1981
11. Vallado DA (2005) An analysis of state vector propagation using differing flight dynamics programs. In: AAS 05-199. AAS/AIAA space flight mechanics conference, Copper Mountain, Colorado
12. Vallado DA (2007) A preliminary analysis of state vector prediction accuracy. In: AAS 07-358. AAS/AIAA space flight mechanics meeting, Sedona, Arizona, 28 January–01 February 2007
13. Chan JC, Navarro D (2001) Comparisons of NORAD two-line elements with INTELSAT orbital elements. In: Proceeding of the third european conference on space debris, Darmstadt, Germany
14. Kelso TS (2007) Validation of SGP4 and IS-GPS-200D against GPS precision ephemerides. In: AAS 07-127. AAS/AIAA space flight mechanics meeting, Sedona, Arizona, 28 January–01 February 2007
15. Boyce WH (2004) Examination of NORAD TLE accuracy using the Iridium constellation. Spaceflight mechanics 2004. Advances Astron Sci 119:2133–2142
16. Snow D, Kaya D (1999) Element set prediction accuracy assessment. Astrodynamics 1999. Advances Astron Sci 103:1937–1958
17. Muldoon AR, Elkaim GH (2008) Improved orbit estimation using GPS measurements for conjunction analysis. In: 21st international technical meeting of the satellite division of the institute of navigation, IONGNSS 2008
18. Zhang JH (1990) Martingale representation of nonlinear system error covariance matrix: an annotation for CADET. J Spacecraft TT&C Technol 1:1–5
19. Han L (2008) Orbit determination and error analysis with space and ground cooperation for LEO space surveillance. National University of Defense Technology, Changsha
20. Junkins J, Akella M, Alfriend K (1996) Non-Gaussian error propagation in orbital mechanics. J Astron Sci 44(4):541–563
21. Yang LP, Zhu YW, Huang H (2010) Planning and control for relative motion trajectory of spacecraft. National Defense Industry Press, Beijing
22. Zhang YK (2002) Study on the technique of satellite formation flying dynamics and control. National University of Defense Technology, Changshang
23. Meng YH (2006) Research on control and application of LEO spacecraft formation flying. National University of Defense Technology, Changsha

24. An XY (2006) Dynamics and application of spacecraft formation flying in eccentric orbits. National University of Defense Technology, Changsha
25. Li JF, Gao YF, Baoyin HX (2002) Study on satellite formation flying dynamics and control. Mech Eng 24(2):1–6
26. Gao YF, Baoyin HX, Li JF (2002) Dynamics behavior and simulation of relative trajectories of satellite formation flying. J Tsinghua Univ (Sci Technol) 42(4):458–461
27. Hill GW (1878) Researches in Lunar theory. Am J Math 1:5–26
28. Clohessy WH, Wiltshire RS (1960) Terminal guidance system for satellite rendezvous. J Aerosp Sci 27(9):653–674
29. Yamanaka K, Ankersen F (2002) New state transition matrix for relative motion on an arbitrary elliptical orbit. J Guid Control Dyn 25(1):60–66
30. Yue XK, Yuan YX (2011) Transfer matrix for relative dynamics in elliptic orbit. Chinese Space Sci Technol 1:42–47
31. Xing JJ (2007) Study on formation design and stationkeeping of spacecraft formation flying. National University of Defense Technology, Changsha
32. Xing JJ, Tang GJ, Xi XN et al (2007) Satellite formation design and optimal station keeping considering nonlinearity and eccentricity. J Guid Control Dyn 30(5):1523–1528
33. Xing JJ, Li HY, Tang GJ et al (2006) Periodic relative motion condition for satellites formations considering nonlinearity. J Astronaut 27(3):359–362
34. Xing JJ, Tang GJ, Xi XN et al (2006) Nonlinear and periodic relative motion in spacecraft formations in eccentric orbits. J Tsinghua Univ (Sci Technol) 46(8):1462–1465
35. Xing JJ, Tang GJ, Li HY (2006) New method of the analytic periodic solution for spacecraft formation in elliptical orbits. In: 57th international astronautical congress, Spain
36. Xing JJ, Li HY, Tang GJ et al (2006) Periodic-relative rotating orbits design for spacecraft formations by numerical optimization. J National Univ Defense Technol 28(1):13–16
37. Xing JJ, Hao XN, Wang W et al (2003) Relative states autonomous determination of two satellites formation. J Astronaut 24(3):254–258
38. Chen L, Han L, Bai XZ et al (2010) Orbital dynamics and error analysis of space target. National Defense Industry Press, Beijing
39. Chan FK (2008) Spacecraft collision probability. The Aerospace Press, El Segundo
40. Alfriend KT, Akella MR, Frisbee J et al (1999) Probability of collision error analysis. Space Debris 1:21–35
41. Ghrist RW,Plakalovic D (2012) Impact of non-Gaussian error volumes on conjunction assessment risk analysis. In: AIAA 2012-4965. AIAA/AAS astrodynamics specialist conference, Minneapolis, Minnesota
42. Bai XZ (2008) Research on collision probability in space objects collision detection. National University of Defense Technology, Changsha
43. Liu ZG (2011) Relativity of satellite orbit error. J Spacecraft TT&C Technol 30(5):45–49
44. Schaub H, Alfriend KT (2002) Hybrid Cartesian and orbit element feedback law for formation flying spacecraft. J Guid Control Dyn 25(2):387–393
45. Schaub H (2004) Relative orbit geometry through classical orbit element differences. J Guid Control Dyn 27(5):839–848
46. Ma ZH (2000) Handbook of modern applied mathematics: volume for probability statistics and stochastic process. Tsinghua University Press, Beijing

http://www.springer.com/978-981-10-2962-2

Orbital Data Applications for Space Objects
Conjunction Assessment and Situation Analysis
Chen, L.; Bai, X.-Z.; Liang, Y.-G.; Li, K.-B.
2017, XXIV, 318 p. 176 illus., 115 illus. in color.,
Hardcover
ISBN: 978-981-10-2962-2